ON THE ELASTIC PROPERTIES OF THE EQUIVALENT TRANSVERSELY ISOTROPIC MATERIAL

ON THE ELASTIC PROPERTIES OF THE EQUIVALENT TRANSVERSELY ISOTROPIC MATERIAL

By

FARHAD VATANDOOST

Submitted to the Department of Civil Engineering
in Partial Fulfillment of the Requirements
for the Degree

Master of Engineering

McMaster University

MASTER OF ENGINEERING (2009) **McMaster University**
(Engineering) **Hamilton, Ontario**

TITLE: **On the elastic properties of the equivalent transversely isotropic material**

AUTHOR: **Farhad Vatandoost**

SUPERVISORS: Professor D. Stolle

NUMBER OF PAGES: xiii, 73

ABSTRACT

The subject of this study is the mechanical response of soil masses consisting of numerous strata in their elastic range. The study comprises analytical, experimental and numerical aspects and provides an insight to the concept of 'equivalent' homogeneous cross-anisotropic material indicating that a system of strata can be replaced by an equivalent transversely isotropic material.

The elastic material properties of such an equivalent transversely isotropic are derived analytically, based on the elastic constants of the constituents. The experimental study is carried out to investigate and verify the concept of the equivalent transversely isotropic material. The experiments involve triaxial tests on samples of two types of homogeneous clay, as well as tests on layered samples consisting of the homogeneous materials. In the numerical part of the study, the tests conducted in the experiments, were simulated via finite element analysis. A comparison is made between the elastic constants obtained from the mathematical formulation, the experiments and FE simulations.

Acknowledgements

First, I would like to thank my supervisor Dr. D. Stolle for accepting me as his MEng. student in McMaster University and giving me the great opportunity to enhance my knowledge. Without his excellent guidance, engagement, encouragement and wisdom, it would have been so much harder to conduct this work.

I would like to thank my friend Alireza Azami for all the wonderful time that we shared and their help and advices during my project.

I would like to thank our geotechnical laboratory technician Peter Koudys for his great advices and help during my experimental work.

My especial thanks are belong to my wife, Sara who this work is truly because of her, who gave me the best gift in my life, our son Milad, who without her patient and encouragement this work was impossible to accomplish.

My final thanks belong to my son Milad, who sparked in my life and brought joy and happiness.

In closing, I thank God. For only through God's grace and blessings has this pursuit been possible.

TABLE OF CONTENTS

LIST OF ILLUSTRATIONS

LIST OF TABLES

CHAPTER 1
INTRODUCTION

1.1 Problem Statement

Natural soils and sedimentary rocks often have roots in sedimentation processes as they are typically formed by deposition and progressive consolidation during their formation. They usually have a distinct internal structure, which is characterized by the appearance of multiple layers or bedding planes. As a result, the mechanical characteristics display an inherent anisotropy. Typical examples of such materials include limestone and mudstone. The primary manifestation of the microstructure on a larger scale is the anisotropy of the mechanical properties, in both elastic and inelastic ranges (e.g. Oda et al. 1978, Yamada and Ishihara 1979, Lo and Hori 1979, Graham and Houlsby 1983, Kirkgard and Lade 1991, Niandou et al. 1997, Duveau et al. 1998, Oka et al. 2002, Nishimura et al. 2007).

In practice, many geotechnical projects involve rock or soil masses consisting of numerous strata on which loads of various kinds, either normal, shear or rotational, are applied, or in which excavations are made. Most often, it is an extremely complex operation to take into account the individual properties of each of these strata in a stress-strain or stability analysis. The complexity comes from considering anisotropic behavior for each individual layer, and also using a very fine spatial discretization. Even with advanced computers and the available computational tools it is too costly to perform such

an analysis. Under certain conditions, however, a system of strata can be replaced by an 'equivalent' homogeneous cross-anisotropic material (Salamon 1968) that considerably simplifies any analysis or prediction of behavior. These conditions are (Wardle and Gerrard 1972):

1- each of the layers are bounded by parallel planes and consist of homogeneous elastic cross-anisotropic material with the axis of symmetry being normal to the bounding planes

2- all interface planes between layers remain in contact and are fully continuous in the sense that no relative displacements occur between the layers at the interface

3- the REV (representative element volume) of the stratified mass, on the basis of which the *equivalent homogeneous* properties are calculated, must on one hand contain a large number of layers and on the other hand the length of such a representative sample, in the direction perpendicular to the bounding plane, must be much smaller than the characteristic length of the excavation or load associated with the particular problem

The properties of the equivalent homogeneous material, usually calculated by a homogenization technique (averaging), has some shortcomings:

1- layers which require completely different structure of constitutive relations may render averaging difficult because incompatible sets of parameters are used for each layer.

2- generally, neither stiffness nor compliance can be averaged.

3- a very thin and weak layer may often facilitate failure. Such layers, however, have little influence on average parameters if the thickness of the layer is taken as a weighting factor.

In elastic soil models, at a wide variety of scales, the subsurface is a layered sequence of different constituent media. It is therefore important to understand the elastic properties of such a sequence, in particular for determining the response of a layered medium to seismic waves. It can be shown that if the individual layer thicknesses are much less than the wavelength of a seismic wave passing through the stack, the wave will propagate as though it were traversing a homogenous, anisotropic medium (Postma, 1955). This property has been subjected to rigorous testing both experimentally (Melia and Carlson, 1984) and numerically (Carcione et al., 1991). The elastic properties of this "equivalent medium" can be derived algebraically from the elastic properties of the materials that comprise the layers (Backus, 1962). The homogenous equivalent medium will be transversely isotropic, the axis of symmetry lying perpendicular to the layering.

1.2 Scope of the Work

This report is structured as follows. Chapter 2 presents a brief review of elastic constitutive models. It also presents an introduction on the equivalent transversely isotropic material, consisting of layers of isotropic materials. The experimental program of the study is presented in Chapter 3. This involves describing the materials used in the investigation, sample preparation techniques, testing methods/setups, the equipments used and the obtained results and observations. Data Analysis and verification of analytical and experimental results are presented in Chapter 4. Mechanical response of the equivalent transversely isotropic material is also simulated in Finite Element analyses. A comparison between the experimental, analytical and numerical results concludes

Chapter 4. Conclusions and recommendations for future work are presented in the last Chapter.

CHAPTER 2
LITERATURE REVIEW

2.1 Introduction

Elastic constitutive equations for isotropic, orthotropic and cross anisotropic (transversely isotropic) materials are reviewed in this chapter. The homogenization equations to find the properties of the equivalent homogeneous medium consisting of layers of different material are also presented.

2.2 Definition of an Elastic Material

There are both physical and mathematical definitions of an elastic material. If under applied loads a material stores but does not dissipate energy, and it returns to its original shape when the loads are removed, we call such a material elastic. This is the physical definition of an elastic material. If a strain energy or elastic potential function can be defined for a material, and the stress state in the material can be obtained by differentiating the strain energy function, such a material can also be called elastic (e.g. Timoshenko and Goodier 1970, Saada 1993). This last definition can be attributed to George Green, an English mathematician (1791-1840). We can see that the mathematical definition of an elastic material is related to the physical definition. The main physical characteristic of a purely elastic material is that it stores "strain" energy due to a load. Mathematically, an elastic material is one, for which a strain energy function can be defined. The strain energy function depends both on strains and on constants that must be

experimentally determined. Thus, for the case of small deformation, the stress tensor (σ_{ij}) can be obtained from the small strain tensor (ε_{ij}), via the potential function W as

$$\sigma_{ij} = \frac{\partial W}{\partial \varepsilon_{ij}} \tag{2.1}$$

For a linear elastic medium the strain energy is a quadratic expansion in terms of the strain tensor ε_{ij}; i.e.

$$W = \frac{1}{2} D_{ijkl} \varepsilon_{ij} \varepsilon_{kl} \tag{2.2}$$

where D_{ijkl} is the fourth order elastic constitutive tensor.

2.3 Generalized Hooke's Law

For a large number of solids, the measured strain is proportional to the load over a wide range of loads, which means that when the load increases, the measured strain increases in the same ratio. Also when the load is reduced to zero, the strain disappears. These experimental facts lead by inductive reasoning to the generalized Hooke's law of the proportionality of the stress and strain. The general form of the law is expressed by the statement: each of the components of the state of stress at a point is a linear function of the components of the state of strain at the point. Mathematically, this is expressed by

$$\sigma_{ij} = \frac{\partial W}{\partial \varepsilon_{ij}} = D_{ijkl} \varepsilon_{kl} \tag{2.3}$$

Given the 81 constants (for the 3D cases), it is fortunately possible to reduce the number of constants taking into account symmetry. Considering first, the symmetry in the stress tensor

$$\sigma_{ij} = D_{ijkl}\varepsilon_{kl} = \sigma_{ji} = D_{jikl}\varepsilon_{kl} \tag{2.4}$$

we have,

$$D_{ijkl} = D_{jikl} \tag{2.5}$$

and the first pair of indices can be freely interchanged. Using the symmetry of the strain tensor and some mathematical manipulations, it is possible to prove that the second pair of indices can be freely interchanged. This reduces the 81 elastic constants to 36.

The existence of the strain energy function facilitates a further simplification of Hooke's law. According to equation (2.2) in general one can write

$$\frac{\partial W}{\partial \varepsilon_{ij}\partial \varepsilon_{kl}} = \frac{\partial W}{\partial \varepsilon_{kl}\partial \varepsilon_{ij}} = D_{ijkl} = D_{klij} \tag{2.6}$$

This shows that the elastic constitutive tensor is symmetric. Accordingly, the number of independent elastic coefficients for the general anisotropic linearly elastic material is reduced to 21. The elastic constitutive relation, with its 21 independent constants, can be written in matrix notation as

$$\begin{Bmatrix} \sigma_{11} \\ \sigma_{22} \\ \sigma_{33} \\ \sigma_{12} \\ \sigma_{13} \\ \sigma_{23} \end{Bmatrix} = \begin{bmatrix} D_{1111} & D_{1122} & D_{1133} & D_{1112} & D_{1113} & D_{1123} \\ & D_{2222} & D_{2233} & D_{2212} & D_{2213} & D_{2223} \\ & & D_{3333} & D_{3312} & D_{3313} & D_{3323} \\ & & & D_{1212} & D_{1213} & D_{1223} \\ & Sym. & & & D_{1313} & D_{1323} \\ & & & & & D_{2323} \end{bmatrix} \begin{Bmatrix} \varepsilon_{11} \\ \varepsilon_{22} \\ \varepsilon_{33} \\ \varepsilon_{12} \\ \varepsilon_{13} \\ \varepsilon_{23} \end{Bmatrix} \tag{2.7}$$

2.4 Elastic Symmetry

A type of symmetry is expressed by the statement that the coefficients D_{ijkl} remain invariant under a transformation of coordinates. Following Saada 1993, the cases considered here are

1) symmetry with respect to a plane

2) symmetry with respect to two mutually perpendicular planes

3) symmetry of rotation with respect to one axis

4) symmetry of rotation with respect to two mutually perpendicular axes, in other words isotropy

If we consider that the transformation tensor, which consists of the direction cosines of the new coordinate system relative to the old one, to be R_{ij}, i.e $x_i' = R_{ij}x_j$, the transformed the elastic constitutive tensor D'_{pqrs} can be found as

$$D'_{pqrs} = R_{pi}R_{qj}R_{rk}R_{sl}D_{ijkl} \tag{2.8}$$

2.4.1 Symmetry with Respect to One Plane

A material that exhibits symmetry of its elastic properties with respect to one plane is called a monoclinic material. Considering that plane is $ox_1 - ox_2$ in Fig. 2-1, this symmetry is expressed by the requirement that the elastic constants do not change under a change from the system (x_1, x_2, x_3) to the system (x_1', x_2', x_3'). The corresponding transformation tensor is

$$\mathbf{R} = \begin{pmatrix} 1 & 0 & 0 \\ 0 & 1 & 0 \\ 0 & 0 & -1 \end{pmatrix} \tag{2.9}$$

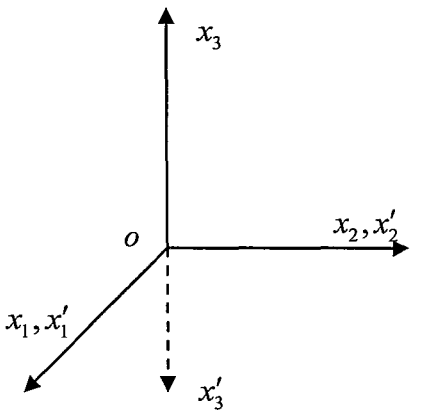

Fig. 2-1 Systems of coordinates for analyzing a monoclinic material

From the symmetry, the term D'_{1123} should be equal to D_{1123}. Substituting $\mathbf{R}$, defined in Eqn. (2.9), into Eqn. (2.8) leads to

$$D'_{1123} = R_{1i}R_{1j}R_{2k}R_{3l}D_{ijkl} = -D_{1123} \tag{2.10}$$

This is only possible when $D'_{1123} = D_{1123} = 0$. A similar reasoning for D_{1113}, D_{2213}, D_{2223}, D_{3313}, D_{3323}, D_{1213} and D_{1223} shows that the number of elements of the stiffness matrix is reduced to 13. The resulting matrix can be written as

$$\begin{bmatrix} D_{1111} & D_{1122} & D_{1133} & D_{1112} & 0 & 0 \\ & D_{2222} & D_{2233} & D_{2212} & 0 & 0 \\ & & D_{3333} & D_{3312} & 0 & 0 \\ & & & D_{1212} & 0 & 0 \\ & Sym. & & & D_{1313} & D_{1323} \\ & & & & & D_{2323} \end{bmatrix} \tag{2.11}$$

2.4.2 Symmetry with Respect to Two Orthogonal Planes

A material which exhibits symmetry of its elastic properties with respect to two orthogonal planes is called an orthotropic material. Considering that planes $ox_1 - ox_2$ and $ox_2 - ox_3$ are the planes of symmetry in Fig. 2-2, this symmetry is expressed by the requirement that the elastic constants do not change under a change from the system (x_1, x_2, x_3) to the system (x'_1, x'_2, x'_3). The corresponding transformation tensor becomes

$$\mathbf{R} = \begin{pmatrix} -1 & 0 & 0 \\ 0 & 1 & 0 \\ 0 & 0 & -1 \end{pmatrix} \tag{2.12}$$

Similar to the case of monoclinic material, considering the symmetry and the transformation law simultaneously reveals that some more terms of the elastic

constitutive tensor are equal to zero. The number of elastic constants is then reduced to 9, as shown in the matrix that follows

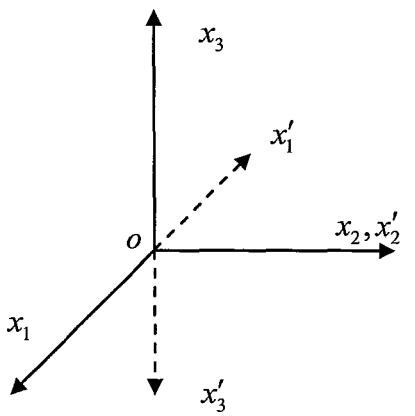

Fig. 2-2 Systems of coordinates for analyzing an orthogonal material

$$\begin{bmatrix} D_{1111} & D_{1122} & D_{1133} & 0 & 0 & 0 \\ & D_{2222} & D_{2233} & 0 & 0 & 0 \\ & & D_{3333} & 0 & 0 & 0 \\ & & & D_{1212} & 0 & 0 \\ & Sym. & & & D_{1313} & 0 \\ & & & & & D_{2323} \end{bmatrix} \tag{2.13}$$

2.4.3 Symmetry of Rotation with Respect to One Axis

A material that possesses one axis of symmetry, in the sense that all rays at right angles to this axis are equivalent, is called transversely isotropic or cross anisotropic. The symmetry is expressed by the requirement that the elastic constants are unaltered in any rotation θ around the axis of symmetry (Fig. 2-3). Taking ox_3 as the axis of symmetry, the direction cosines and the transformation tensor are

$$\mathbf{R}=\begin{pmatrix}\cos\theta & \sin\theta & 0\\ -\sin\theta & \cos\theta & 0\\ 0 & 0 & 1\end{pmatrix} \tag{2.14}$$

Starting from the elastic constitutive equation, Eqn. (2.3), for both systems of coordinates one can write

$$\sigma_{ij}=D_{ijkl}\varepsilon_{kl} \quad ; \quad \sigma'_{ji}=D_{jikl}\varepsilon'_{kl} \tag{2.15}$$

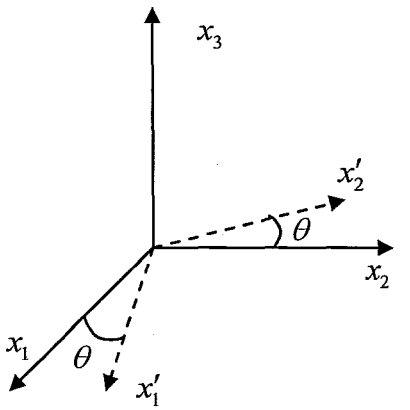

Fig. 2-3 Systems of coordinates for analyzing a transversely isotropic material

For a rotation of axes around ox_3 the strain state in (x'_1, x'_2, x'_3) is expressed as

$$\begin{aligned}
\varepsilon'_{11} &= \varepsilon_{11}\cos^2\theta + 2\varepsilon_{12}\cos\theta\sin\theta + \varepsilon_{22}\sin^2\theta\\
\varepsilon'_{22} &= \varepsilon_{11}\sin^2\theta - 2\varepsilon_{12}\cos\theta\sin\theta + \varepsilon_{22}\cos^2\theta\\
\varepsilon'_{33} &= \varepsilon_{33}\\
\varepsilon'_{12} &= (\varepsilon_{22}-\varepsilon_{11})\cos\theta\sin\theta + \varepsilon_{12}(\cos^2\theta - \sin^2\theta)\\
\varepsilon'_{13} &= \varepsilon_{13}\cos\theta + \varepsilon_{23}\sin\theta\\
\varepsilon'_{23} &= -\varepsilon_{13}\sin\theta + \varepsilon_{23}\cos\theta
\end{aligned} \tag{2.16}$$

The components of the stress tensor transform exactly in the same way. Considering that $\sigma'_{33} = \sigma_{33}$, then from Eqn. (2.15) one can write

$$\begin{aligned} \sigma'_{33} &= D_{3311}\varepsilon'_{11} + D_{3322}\varepsilon'_{22} + D_{3333}\varepsilon'_{33} + 2(D_{3312}\varepsilon'_{12} + D_{3313}\varepsilon'_{13} + D_{3323}\varepsilon'_{23}) = \\ \sigma_{33} &= D_{3311}\varepsilon_{11} + D_{3322}\varepsilon_{22} + D_{3333}\varepsilon_{33} + 2(D_{3312}\varepsilon_{12} + D_{3313}\varepsilon_{13} + D_{3323}\varepsilon_{23}) \end{aligned} \tag{2.17}$$

Substituting the values for ε'_{ij} from Eqn. (2.16) into Eqn. (2.17), one can find

$$\begin{aligned} &D_{3311}\left(\varepsilon_{11}\cos^2\theta + 2\varepsilon_{12}\cos\theta\sin\theta + \varepsilon_{22}\sin^2\theta\right) + \\ &D_{3322}\left(\varepsilon_{11}\sin^2\theta - 2\varepsilon_{12}\cos\theta\sin\theta + \varepsilon_{22}\cos^2\theta\right) + \\ &D_{3333}\varepsilon'_{33} + 2D_{3312}\left((\varepsilon_{22} - \varepsilon_{11})\cos\theta\sin\theta + \varepsilon_{12}(\cos^2\theta - \sin^2\theta)\right) + \\ &2D_{3313}\left(\varepsilon_{13}\cos\theta + \varepsilon_{23}\sin\theta\right) + 2D_{3323}\left(-\varepsilon_{13}\sin\theta + \varepsilon_{23}\cos\theta\right) = \\ &D_{3311}\varepsilon_{11} + D_{3322}\varepsilon_{22} + D_{3333}\varepsilon_{33} + 2(D_{3312}\varepsilon_{12} + D_{3313}\varepsilon_{13} + D_{3323}\varepsilon_{23}) \end{aligned} \tag{2.18}$$

Equating to zero the sum of the coefficients of ε_{11} in the above relation, one can find that for all values of θ,

$$\left(D_{3311} - D_{3322}\right)\sin^2\theta + 2D_{3312}\sin\theta\cos\theta = 0 \tag{2.19}$$

from which it follows that

$$D_{3311} = D_{3322} \;\; ; \;\; D_{3312} = 0 \tag{2.20}$$

Considering ε_{22} and ε_{12}, leads to the same results. Equating the sum of the coefficients of ε_{13} and ε_{23} to zero results in

$$D_{3313} = D_{3323} = 0 \tag{2.21}$$

Similar manipulations can be performed for σ_{13} and σ'_{13}, and once again by considering the sum of the coefficients of ε_{11}, it can be concluded that

$$D_{1311} = D_{1322} = D_{1312} = D_{2311} = 0 \tag{2.22}$$

The sum of the coefficients of ε_{12}, when equated to zero, leads to

$$D_{1311} = D_{1322} \;\; ; \;\; D_{1312} = D_{2312} = 0 \tag{2.23}$$

while the sum of the coefficients of ε_{13} yields the relation

$$D_{2313} = 0 \tag{2.24}$$

Repeating the steps for σ_{11} and σ'_{11}, one can find, after equating to zero the sum of the coefficients of ε_{11}, ε_{22} and ε_{33}, that

$$D_{1211} = D_{1233} = 0 \;\; ; \;\; D_{1133} = D_{2233} \;\; ; \;\; D_{1111} = D_{2222} \tag{2.25}$$

The sum of the coefficients of ε_{12}, when equated to zero, yields

$$D_{1212} = \frac{1}{2}\left(D_{1111} - D_{1122}\right) \;\; ; \;\; D_{1222} = 0 \tag{2.26}$$

Finally, considering the sum of the coefficients of ε_{13} in the equation obtained from σ_{23} and σ'_{23}, we get

$$D_{2323} = D_{1313} \tag{2.27}$$

The constitutive matrix, with its five remaining independent constants, can now be simplified to

$$\begin{bmatrix} D_{1111} & D_{1122} & D_{1133} & 0 & 0 & 0 \\ & D_{1111} & D_{1133} & 0 & 0 & 0 \\ & & D_{3333} & 0 & 0 & 0 \\ & & & \frac{1}{2}(D_{1111} - D_{1122}) & 0 & 0 \\ & Sym. & & & D_{1313} & 0 \\ & & & & & D_{1313} \end{bmatrix} \tag{2.28}$$

2.4.4 Isotropy

An isotropic material possesses elastic properties that are independent of the orientation of the axes. In other words, it is a material which possesses a rotational symmetry with respect to two perpendicular axes. By repeating the argument of the previous subsection, one obtains

$$D_{1213} = \frac{1}{2}(D_{1111} - D_{1122}) = 0 \;;\; D_{3333} = D_{1111} \;;\; D_{1133} = D_{1122} \tag{2.29}$$

so that, there are only 2 independent terms remaining in the constitutive matrix

$$\begin{bmatrix} D_{1111} & D_{1122} & D_{1122} & 0 & 0 & 0 \\ & D_{1111} & D_{1122} & 0 & 0 & 0 \\ & & D_{1111} & 0 & 0 & 0 \\ & & & \frac{1}{2}(D_{1111}-D_{1122}) & 0 & 0 \\ & Sym. & & & \frac{1}{2}(D_{1111}-D_{1122}) & 0 \\ & & & & & \frac{1}{2}(D_{1111}-D_{1122}) \end{bmatrix} \quad (2.30)$$

The elastic coefficients in Eqn. (2.30) are often expressed using Lame's constants (λ, μ)

$$D_{1122} = \lambda \;;\; D_{1212} = \frac{1}{2}(D_{1111} - D_{1122}) = \mu \;;\; D_{1111} = \lambda + \mu \quad (2.31)$$

$$\begin{bmatrix} \lambda+\mu & \lambda & \lambda & 0 & 0 & 0 \\ & \lambda+\mu & \lambda & 0 & 0 & 0 \\ & & \lambda+\mu & 0 & 0 & 0 \\ & & & \mu & 0 & 0 \\ & Sym. & & & \mu & 0 \\ & & & & & \mu \end{bmatrix} \quad (2.32)$$

and the constitutive equations can be expressed in index notation as

$$\sigma_{ij} = 2\mu\varepsilon_{ij} + \lambda\delta_{ij}\varepsilon_{nn} \quad ; \quad \varepsilon_{ij} = \frac{-\lambda\delta_{ij}}{2\mu(3\lambda+2\mu)}\sigma_{nn} + \frac{1}{2\mu}\sigma_{ij} \quad (2.33)$$

where $\delta_{ij} = 1$ if $i = j$ and $\delta_{ij} = 0$ otherwise.

The two independent constants most often considered in engineering are however the elastic modulus, E, and Poisson's ratio, ν. Under a uniaxial state of stress σ_{11}

$$\varepsilon_{11} = \frac{\lambda+\mu}{\mu(3\lambda+2\mu)}\sigma_{11} = \frac{\sigma_{11}}{E}$$
$$\varepsilon_{22} = \frac{-\lambda}{2\mu(3\lambda+2\mu)}\sigma_{11} = -\frac{\nu}{E}\sigma_{11} \qquad (2.34)$$
$$\varepsilon_{33} = \frac{-\lambda}{2\mu(3\lambda+2\mu)}\sigma_{11} = -\frac{\nu}{E}\sigma_{11}$$

Poisson's ratio is thus the ratio between the lateral contraction and the axial elongation under a uniaxial stress condition. From Eqn. (2.34) elastic modulus and the Poisson's ration are

$$E = \frac{\mu(3\lambda+2\mu)}{\lambda+\mu} \quad ; \quad \nu = \frac{\lambda}{2(\lambda+\mu)} \qquad (2.35)$$

2.5 Equivalent Transversely Isotropic Material

The elastic constitutive model for transversely isotropic material was presented in the previous subsection. This type of material has 5 independent constants. In terms of elastic modulus and Poisson's ratio, with five independent variables of $E_h, E_v, \nu_h, \nu_{hv}$ and μ_{hv}, the elastic constants of the constitutive tensor for a transversely isotropic material can be expressed as

$$\begin{aligned}
D_{1111} &= D_{2222} = E_h(1-\nu_{vh}\nu_{hv})\Upsilon \\
D_{3333} &= E_v(1-\nu_h^2)\Upsilon \\
D_{1122} &= E_h(\nu_h+\nu_{vh}\nu_{hv})\Upsilon \\
D_{1133} &= E_h(\nu_{vh}+\nu_{vh}\nu_h)\Upsilon = E_v(\nu_{hv}+\nu_{hv}\nu_h)\Upsilon \\
D_{1212} &= \mu_h \\
D_{1313} &= \mu_{hv}
\end{aligned} \qquad (2.36)$$

where

$$\begin{aligned}
&\Upsilon = (1-\nu_h^2-2\nu_{hv}\nu_{vh}-2\nu_h\nu_{hv}\nu_{vh})^{-1} \\
&\mu_h = \frac{1}{2}(D_{1111}-D_{1122}) = \frac{E_h}{2(1+\nu_h)} \\
&E_h\nu_{vh} = E_v\nu_{hv}
\end{aligned} \tag{2.37}$$

In the above, the symmetry of rotation is around the vertical axis (v) and plane of isotropy is horizontal (h). Poisson's ratio , ν_{ij}, corresponds to a contraction in direction j when an extension is applied in direction i.

As pointed out in the first chapter, the strength and the mechanical behavior of a medium consisting of parallel layers of different materials, under certain conditions can be approximated by an 'equivalent' homogeneous cross-anisotropic material (e.g. Wardle and Gerrard 1972, Brittan et al. 1995, Niemunis et al. 2000, Stolle and Guo 2007, Guo and Stolle 2009). What follows in this subsection is the determination of the material properties of the "equivalent" transversely isotropic material in the elastic range (Salamon 1968).

Fig. 2-4 shows a simple case of a stratified medium consisting of a large number of alternating parallel layers of two homogeneous, isotropic materials for which the elastic behavior of each layer is given by Lame's constants (λ_1,μ_1), and (λ_2,μ_2), respectively. The layer thickness for the first material is d_1; for the second is d_2. The z-axis is taken perpendicular to and the x and y axes that are parallel to the layers. The height of the parallelepiped is $n(d_1+d_2)$, where n is an integer, providing a RVE with length and width of a and b, respectively.

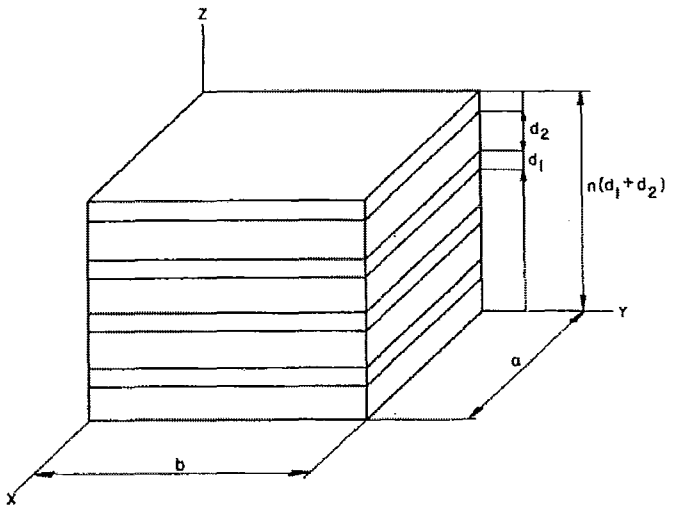

Fig. 2-4 Schematic of an idealized stratified medium

To find the properties of the equivalent transversely isotropic medium, the behavior of the system shown in Fig. 2-4 should be analyzed for various loading conditions. Suppose that on the faces perpendicular to the z axis a normal traction Z_z, is exerted and that there are no tangential components $Z_x = Z_y = 0$. On the faces perpendicular to the x-axis also consider only normal tractions, X_{x1} on the layers (1) and X_{x2} on the layers (2). Similarly, on the faces perpendicular to the y-axis assume normal tractions Y_{y1} and Y_{y2}.The normal tractions X and Y, are such that $\varepsilon_{xx1} = \varepsilon_{xx2} = \varepsilon_{xx}$ and $\varepsilon_{yy1} = \varepsilon_{yy2} = \varepsilon_{yy}$, where ε_{xx1} is the linear dilatation of a line element in the direction of the x-axis in material (1), etc. This restriction is necessary to insure the continuity of the displacement.

From Hooke's law, one can write for materials (1) and (2)

$$
\begin{aligned}
X_{x1} &= (\lambda_1 + 2\mu_1)\varepsilon_{xx} + \lambda_1\varepsilon_{yy} + \lambda_1\varepsilon_{zz1} \\
Y_{y1} &= \lambda_1\varepsilon_{xx} + (\lambda_1 + 2\mu_1)\varepsilon_{yy} + \lambda_1\varepsilon_{zz1} \\
Z_z &= \lambda_1\varepsilon_{xx} + \lambda_1\varepsilon_{yy} + (\lambda_1 + 2\mu_1)\varepsilon_{zz1}
\end{aligned} \qquad (2.38)a
$$

$$
\begin{aligned}
X_{x2} &= (\lambda_2 + 2\mu_2)\varepsilon_{xx} + \lambda_2\varepsilon_{yy} + \lambda_2\varepsilon_{zz2} \\
Y_{y2} &= \lambda_2\varepsilon_{xx} + (\lambda_2 + 2\mu_2)\varepsilon_{yy} + \lambda_2\varepsilon_{zz2} \\
Z_z &= \lambda_2\varepsilon_{xx} + \lambda_2\varepsilon_{yy} + (\lambda_2 + 2\mu_2)\varepsilon_{zz2}
\end{aligned} \qquad (2.38)b
$$

In above the traction on the face perpendicular to the z -axis is Z_z. The average tractions on a face perpendicular to the x and y become

$$
X_x = \frac{d_1 X_{x1} + d_2 X_{x2}}{d_1 + d_2} \;\; ; \;\; Y_y = \frac{d_1 Y_{y1} + d_2 Y_{y2}}{d_1 + d_2} \qquad (2.39)
$$

Form Eqn. (2.38), and Eqn. (2.39) one can find

$$
\begin{aligned}
(d_1 + d_2) X_x &= \varepsilon_{xx}\left[d_1(\lambda_1 + 2\mu_1) + d_2(\lambda_2 + 2\mu_2)\right] + \\
&\quad \varepsilon_{yy}\left(d_1\lambda_1 + d_2\lambda_2\right) + \varepsilon_{zz1}\lambda_1 d_1 + \varepsilon_{zz2}\lambda_2 d_2 \\
(d_1 + d_2) Y_y &= \varepsilon_{xx}\left(d_1\lambda_1 + d_2\lambda_2\right) + \varepsilon_{yy}\left[d_1(\lambda_1 + 2\mu_1) + d_2(\lambda_2 + 2\mu_2)\right] + \\
&\quad \varepsilon_{zz1}\lambda_1 d_1 + \varepsilon_{zz2}\lambda_2 d_2 \\
(d_1 + d_2) Z_z &= \varepsilon_{xx}\left(d_1\lambda_1 + d_2\lambda_2\right) + \varepsilon_{yy}\left(d_1\lambda_1 + d_2\lambda_2\right) + \\
&\quad \varepsilon_{zz1} d_1\left(\lambda_1 + 2\mu_1\right) + \varepsilon_{zz2} d_2\left(\lambda_2 + 2\mu_2\right)
\end{aligned} \qquad (2.40)
$$

If ε_{zz}, the overall dilation of a linear element parallel to the z axis, is defined as

$$\varepsilon_{zz} = \frac{d_1\varepsilon_{zz1} + d_2\varepsilon_{zz2}}{d_1 + d_2} \tag{2.41}$$

Then from Eqns. (2.38) and (2.41) one can find

$$\varepsilon_{zz1} = \frac{(d_1+d_2)(\lambda_2+2\mu_2)\varepsilon_{zz} - (\lambda_1-\lambda_2)(\varepsilon_{xx}+\varepsilon_{yy})d_2}{d_1(\lambda_2+2\mu_2)+d_2(\lambda_1+2\mu_1)}$$

$$\varepsilon_{zz2} = \frac{(d_1+d_2)(\lambda_1+2\mu_1)\varepsilon_{zz} + (\lambda_1-\lambda_2)(\varepsilon_{xx}+\varepsilon_{yy})d_1}{d_1(\lambda_2+2\mu_2)+d_2(\lambda_1+2\mu_1)} \tag{2.42}$$

Substituting Eqn. (2.42) into Eqn. (2.40) leads to

$$X_x = \varepsilon_{xx}\frac{(d_1+d_2)^2(\lambda_1+2\mu_1)(\lambda_2+2\mu_2)+d_1d_2\left[\left[(\lambda_1+2\mu_1)-(\lambda_2+2\mu_2)\right]^2-(\lambda_1-\lambda_2)^2\right]}{D}$$
$$+\varepsilon_{yy}\frac{\lambda_1\lambda_2(d_1+d_2)^2+2(d_1\lambda_1+d_2\lambda_2)(\mu_2d_1+\mu_1d_2)}{D}$$
$$+\varepsilon_{zz}\frac{(d_1+d_2)\left[\lambda_1d_1(\lambda_2+2\mu_2)+\lambda_2d_2(\lambda_1+2\mu_1)\right]}{D}$$

$$Y_y = \varepsilon_{xx}\frac{\lambda_1\lambda_2(d_1+d_2)^2+2(d_1\lambda_1+d_2\lambda_2)(\mu_2d_1+\mu_1d_2)}{D}$$
$$+\varepsilon_{yy}\frac{(d_1+d_2)^2(\lambda_1+2\mu_1)(\lambda_2+2\mu_2)+d_1d_2\left[\left[(\lambda_1+2\mu_1)-(\lambda_2+2\mu_2)\right]^2-(\lambda_1-\lambda_2)^2\right]}{D}$$
$$+\varepsilon_{zz}\frac{(d_1+d_2)\left[\lambda_1d_1(\lambda_2+2\mu_2)+\lambda_2d_2(\lambda_1+2\mu_1)\right]}{D}$$

$$Z_z = (\varepsilon_{xx} + \varepsilon_{yy}) \frac{(d_1 + d_2)\left[d_1\lambda_1(\lambda_2 + 2\mu_2) + d_2\lambda_2(\lambda_1 + 2\mu_1)\right]}{D} + \varepsilon_{zz} \frac{(d_1 + d_2)^2(\lambda_1 + 2\mu_1)(\lambda_2 + 2\mu_2)}{D} \tag{2.43}$$

where $D = (d_1 + d_2)\left[d_1(\lambda_2 + 2\mu_2) + d_2(\lambda_1 + 2\mu_1)\right]$.

Following the same approach by applying a tangential traction Y_z to the faces perpendicular to the z-axis, one can write

$$(d_1 + d_2)\varepsilon_{yz} = d_1\varepsilon_{yz1} + d_2\varepsilon_{yz}2 \;\; ; \;\; Y_z = \mu_1\varepsilon_{yz1} = \mu_2\varepsilon_{yz2} \tag{2.44}$$

Thus:

$$(d_1 + d_2)\varepsilon_{yz} = \left(\frac{d_1}{\mu_1} + \frac{d_2}{\mu_2}\right)Y_z \;\; ; \;\; Y_z = \frac{(d_1 + d_2)\mu_1\mu_2}{d_1\mu_2 + d_2\mu_1}\varepsilon_{yz} \tag{2.45}$$

In a similar way

$$(d_1 + d_2)\varepsilon_{xz} = \left(\frac{d_1}{\mu_1} + \frac{d_2}{\mu_2}\right)X_z \;\; ; \;\; X_z = \frac{(d_1 + d_2)\mu_1\mu_2}{d_1\mu_2 + d_2\mu_1}\varepsilon_{xz} \tag{2.46}$$

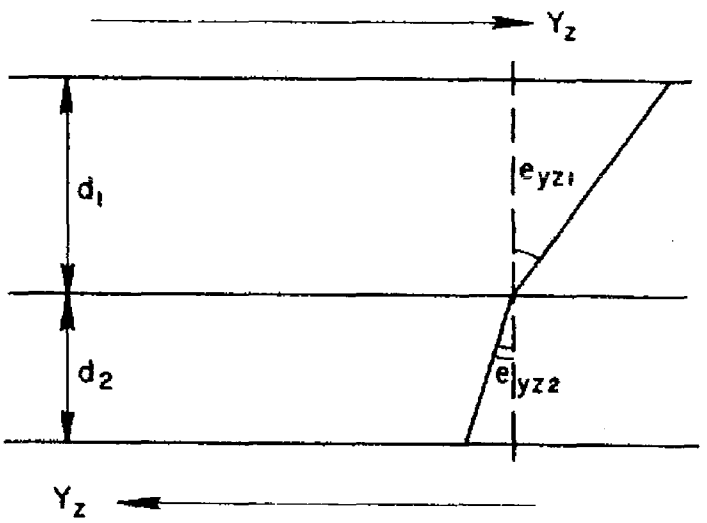

Fig. 2-5 Schematic of an idealized stratified medium (Salamon 1968)

The next step is to apply a tangential force $X_{y1}ad_1$ to the faces perpendicular to the y-axis of the layers of material (1), and a tangential force $X_{y2}ad_2$ to the faces of material (2). Note that ε_{xy1} should be equal to ε_{xy2} to insure the continuity of the displacement. Considering $X_{y1} = \mu_1 \varepsilon_{xy}$ and $X_{y2} = \mu_2 \varepsilon_{xy}$, there is

$$X_y = \frac{X_{y1}d_1 + X_{y2}d_2}{d_1 + d_2} = \frac{(\mu_1 d_1 + \mu_2 d_2)}{d_1 + d_2}\varepsilon_{xy} \tag{2.47}$$

Comparing these results with the constitutive equations for a transversely isotropic material in (2.36) one can conclude that, when viewed on a proper scale, the layered medium may be considered as transversely isotropic medium with the elastic constants as follow

$$D_{1111} = \frac{(d_1+d_2)^2(\lambda_1+2\mu_1)(\lambda_2+2\mu_2)+4d_1d_2(\mu_1-\mu_2)\left[(\lambda_1+\mu_1)-(\lambda_2+\mu_2)\right]}{(d_1+d_2)\left[d_1(\lambda_2+2\mu_2)+d_2(\lambda_1+2\mu_1)\right]}$$

$$D_{3333} = \frac{(d_1+d_2)^2(\lambda_1+2\mu_1)(\lambda_2+2\mu_2)}{(d_1+d_2)\left[d_1(\lambda_2+2\mu_2)+d_2(\lambda_1+2\mu_1)\right]}$$

$$D_{1122} = \frac{(d_1+d_2)^2\lambda_1\lambda_2+2(\lambda_1d_1+\lambda_2d_2)(\mu_1d_2+\mu_2d_1)}{(d_1+d_2)\left[d_1(\lambda_2+2\mu_2)+d_2(\lambda_1+2\mu_1)\right]} \qquad (2.48)$$

$$D_{1133} = \frac{(d_1+d_2)\left[\lambda_1d_1(\lambda_2+2\mu_2)+\lambda_2d_2(\lambda_1+2\mu_1)\right]}{(d_1+d_2)\left[d_1(\lambda_2+2\mu_2)+d_2(\lambda_1+2\mu_1)\right]}$$

$$D_{1313} = \frac{(d_1+d_2)\mu_1\mu_2}{d_1\mu_2+d_2\mu_1} \quad ; \quad D_{1212} = \frac{\mu_1d_1+\mu_2d_2}{d_1+d_2} = \frac{1}{2}(D_{1111}-D_{1122})$$

CHAPTER 3
EXPERIMENTAL PROGRAM

3.1 Introduction

The experimental study to investigate the properties of the "equivalent" transversely isotropic material in the elastic range is presented in this Chapter. This involves selecting and describing the materials used in the investigation, sample preparation techniques, testing methods/setups and the equipment used. The data analysis and the discussion of the results are presented in the chapter that follows.

3.2 Materials

Based on some preliminary tests on some clay, sand and mixed materials, such as Ottawa clay, crushed limestone sand, Dundas clay and kaolinite, the two materials selected for the investigation were brown Dundas clay (passing sieve #25) and kaolinite (passing sieve #50). The layered composite was fabricated by consecutive layering of these two clays. Details of sample preparation are presented later in this Chapter.

Experiments presented here were all performed while keeping track of only total stresses, i.e. the samples were not fully saturated and were prepared at a certain water content. The excess pore water pressure was not measured.

3.3 Image Processing Procedure

For measurements of lateral (horizontal) deformations in the triaxial tests conducted in this study an image processing technique was employed. The axial (vertical) displacement was easily measured by a transducer mounted on the top of the shaft that applied the vertical load. During each test, the vertical displacement was recorded by a data acquisition system and stored to the hard drive of the computer. Simultaneously, the sample was photographed at a constant rate and pictures were also stored to the hard drive of the computer for later image processing. By analyzing the shape of the sample in the photos, via Photoshop, the lateral deformation of the sample could be determined.

Fig. 3-1 shows a 6-layer specimen that was considered for the image processing. To calculate the average horizontal strain, the diameter of each layer was measured at the beginning of the test. The horizontal displacements of the sample for the various layers were then obtained by interpreting the images. The average lateral strain was taken to be the average of the lateral strains of all the layers. The same process was repeated for all specimens. It should be noted that the lateral strains were determined only for those layers in the central portion to eliminate the influence of boundary effects.

3.4 Phase I

Based on the sample preparation technique, the number of the layers in a sample, and testing procedures the experimental study in this work was divided in two phases. Phase I was the preliminary phase, where the elastic range of the materials and the

required stress level were determined, and the sample preparation technique was perfected.

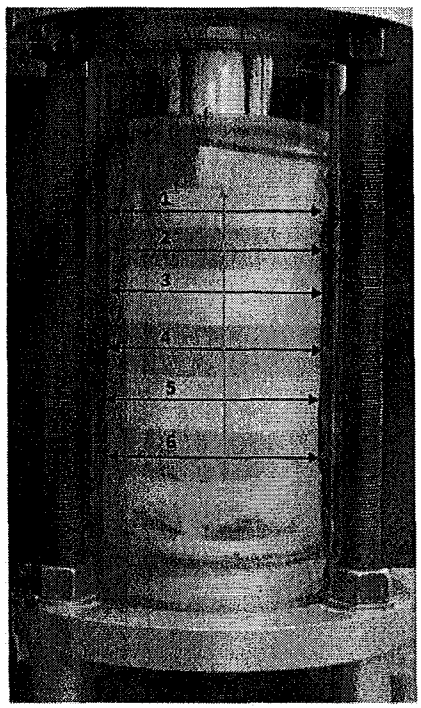

Fig. 3-1 A layered sample in the triaxial cell, measurements of vertical and lateral deformations

3.4.1 Test Specimens

In the early stages to investigate the sample preparation technique, bulk samples of Dundas clay and kaolinite were remolded in a cylindrical mold, 7 cm in diameter and 30 cm high (see Fig. 3-2). The inside of the mold had been sprayed with Teflon to reduce the friction between soil and mold, and thus reduce the sample disturbance during molding and extraction of the sample from the mold. Dundas clay samples with 20%, and kaolinite samples with 14% moisture contents were consolidated in 12 layers of about 2 cm thickness (almost 300g) under an axial stress of 48 kPa. Each layer was kept under

pressure for 5 min. To prevent separation between the layers, the surface of each consolidated layer was scratched with a sharp instrument before adding the next layer. The bulk sample within the mold was then kept under 48 kPa axial stress for an additional consolidation time of 48 hrs.

The bulk samples were then extracted from the mold by a hydraulic jack and cut perpendicular to the axis of the cylinder, to provide the different layers of the sample shown in Fig. 3-3. The layered samples consisted of 6 layers, 3 layers from Dundas clay and the other 3 layers from kaolinite. Thereafter each sample was wrapped in plastic-wrap and placed in the moisture room for another 48 hrs. The layered samples of the type shown in Fig. 3-3, with an approximate height of 10cm, are called Sample A herein.

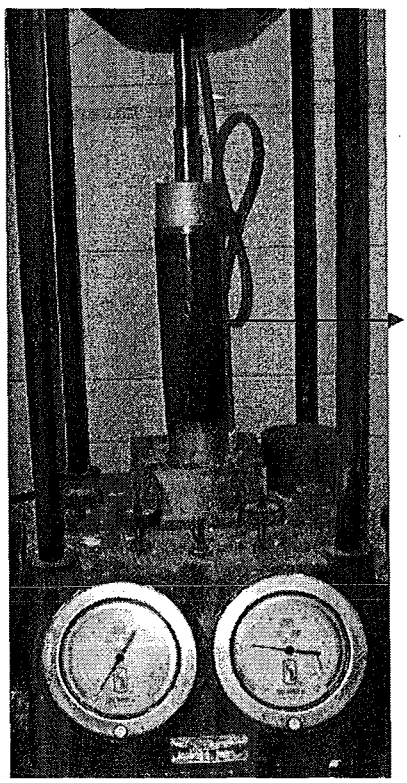

Fig. 3-2 Preparation of bulk samples of Dundas clay and kaolinite

Fig. 3-3 Layered specimens investigated in phase one; consisting 3 layers of Dundas clay and 3 layers of kaolinite; Sample A (7cm in diameter and 10 cm high)

To investigate the behavior of each individual material, the bulk homogeneous samples of Dundas clay and kaolinite were also prepared and examined in triaxial tests.

To simplify the process of sample preparation and to obtain samples with more consistent properties, the sample preparation technique for the layered samples was modified as follows. The process was almost the same as what has been described with the exception that when making the bulk samples of Dundas clay and kaolinite, after compacting each of the 2 cm thickness (almost 300g) layers, a thin layer of fine sand was placed on top of the compacted layer. Presence of the thin layer of sand eliminated the need for cutting the sample and thus reduced the sample disturbance. Also, measurements

of the moisture content within a layer at different location, e.g. at the center and close to the edges, proved that this method helped to provide a material with less variation in the moisture content; see Appendix. Hence the addition of the sand layers both simplified the process and helped obtain layers with more consistent mechanical behavior. A bulk sample of kaolinite prepared with this method is shown in Fig. 3-4. After removing the samples from the moisture room the thin layers of sand were removed and the layers were put back together to form the sample shown in Fig. 3-3.

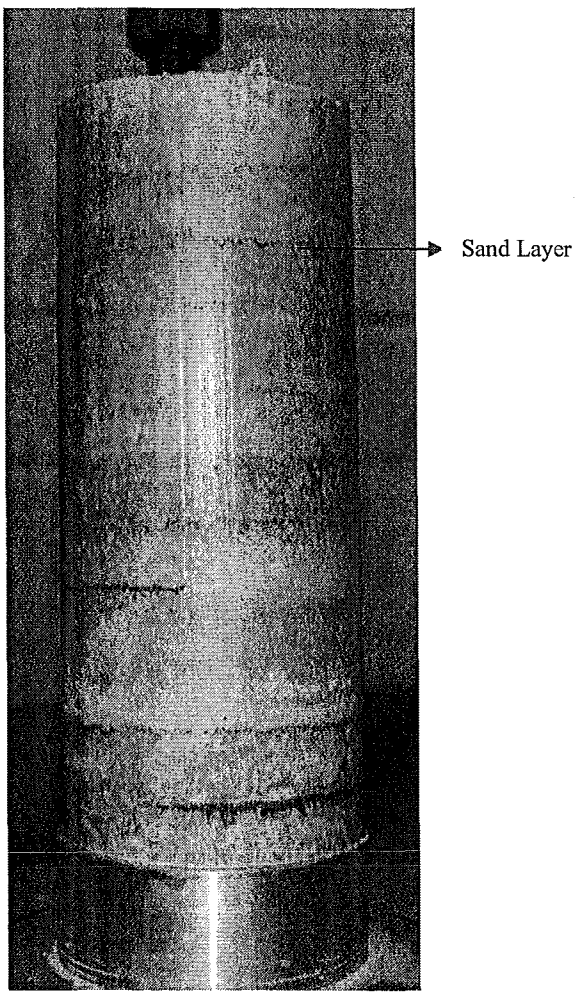

Fig. 3-4 Bulk sample of kaolinite, layers of kaolinite separated by presence of thin layers of sands in between them

3.4.2 Test Setup

After allowing stress relaxation of the samples in the moisture room and allowing them to reach a state of equilibrium, the specimens were subsequently removed from the moisture room and transferred to the base of the triaxial cell and enclosed in a membrane. To minimize the end friction effects two layers of membrane, with silicon grease in between, were placed between the sample and loading platens. Proper cuts were made on the membranes to allow free lateral expansion of the sample. The confining pressure was applied to the sample by controlling the air pressure inside the triaxial cell, and then the sample was failed by applying a vertical displacement via the bottom loading platen.

3.4.3 Experimental Results

The stress-strain and deformation characteristics of the layered and homogeneous samples are presented in Fig. 3-5. The variation of vertical stress and horizontal strain with increasing vertical stress are shown in Fig. 3-5a and Fig. 3-5b, respectively.

From the stress-strain curves in Fig. 3-5a one can observe three distinct stages for each curve. Considering the kaolinite sample, at the axial strain range between 0% to 2% it is clear that the imperfection in the system influences the results and a stiffening is observed that corresponds to the compliance associated with fabrication and seating being eliminated. From 2% to 5% the stress-strain curve resembles a fairly linear behavior, and beyond 5% the plastic behavior dominants until the sample fails. To find the elastic properties of the samples, the linear part of the stress-strain path must be considered, as shown in Fig. 3-6 to Fig. 3-8 .

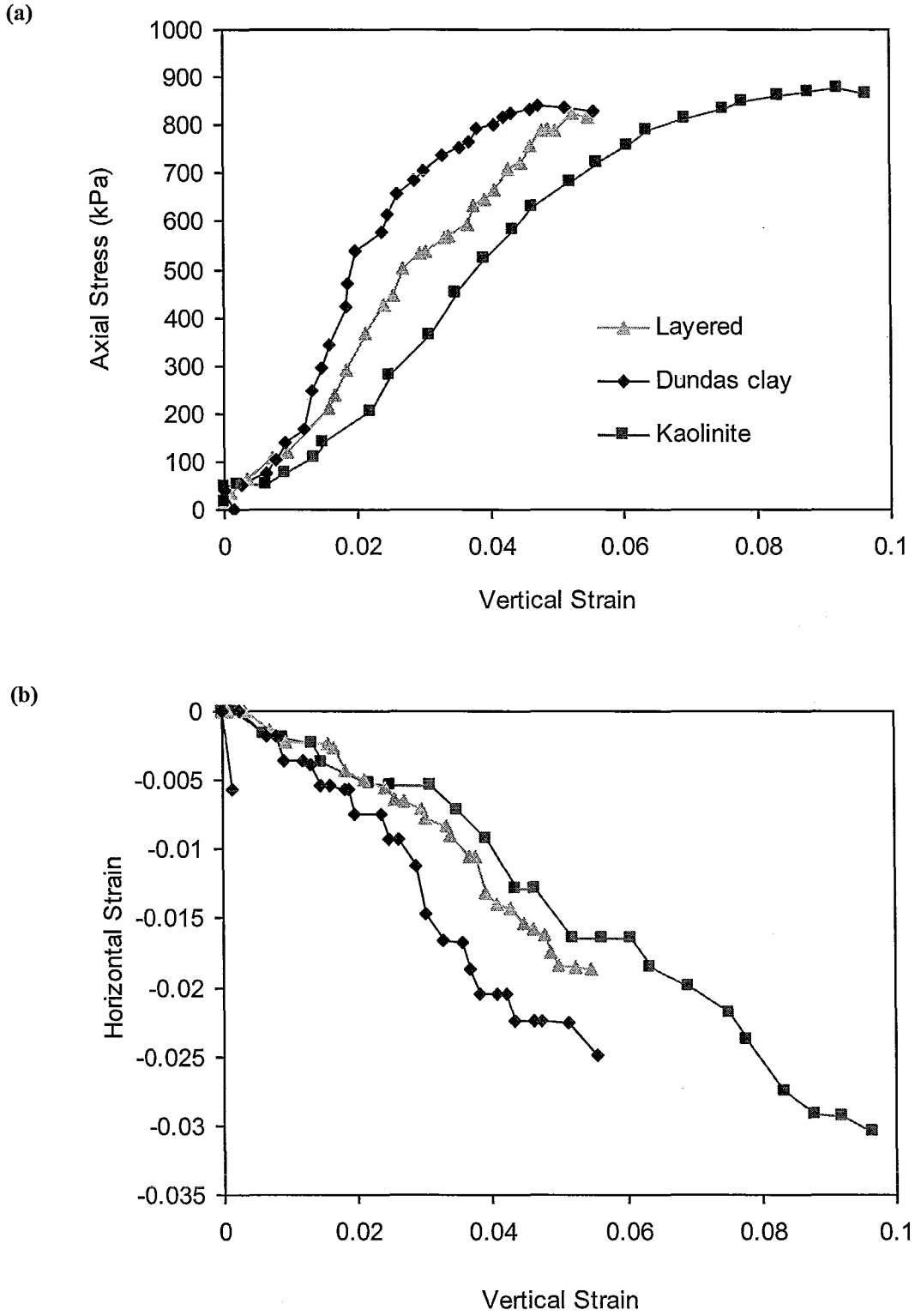

Fig. 3-5 Variation of (a) vertical stress and (b) horizontal strain with vertical strain for the layered, kaolinite and Dundas clay samples

(a)

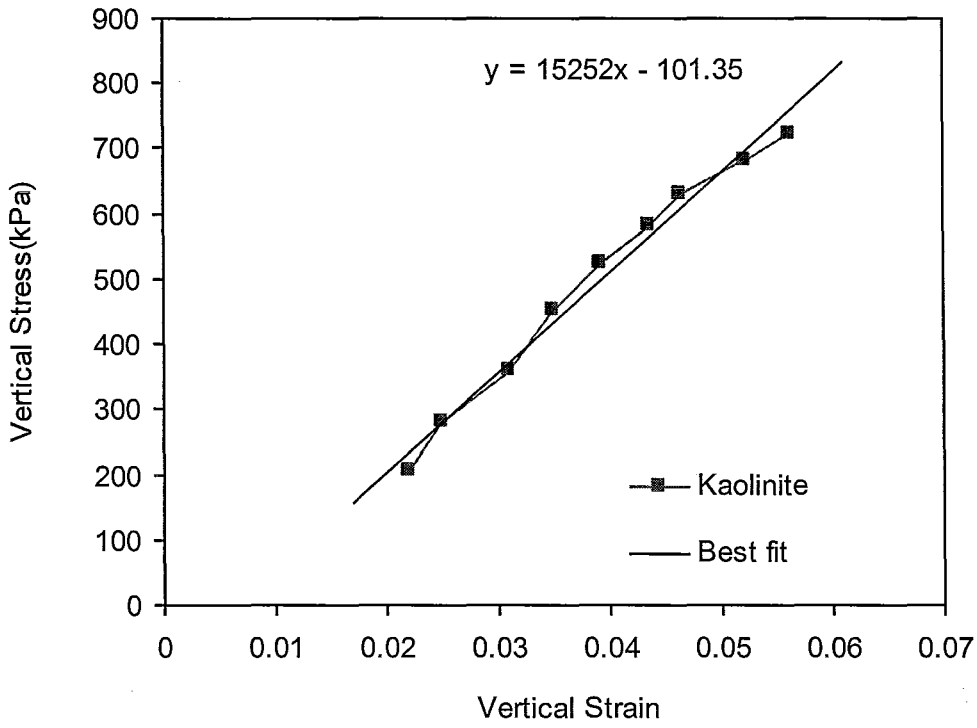

(b)

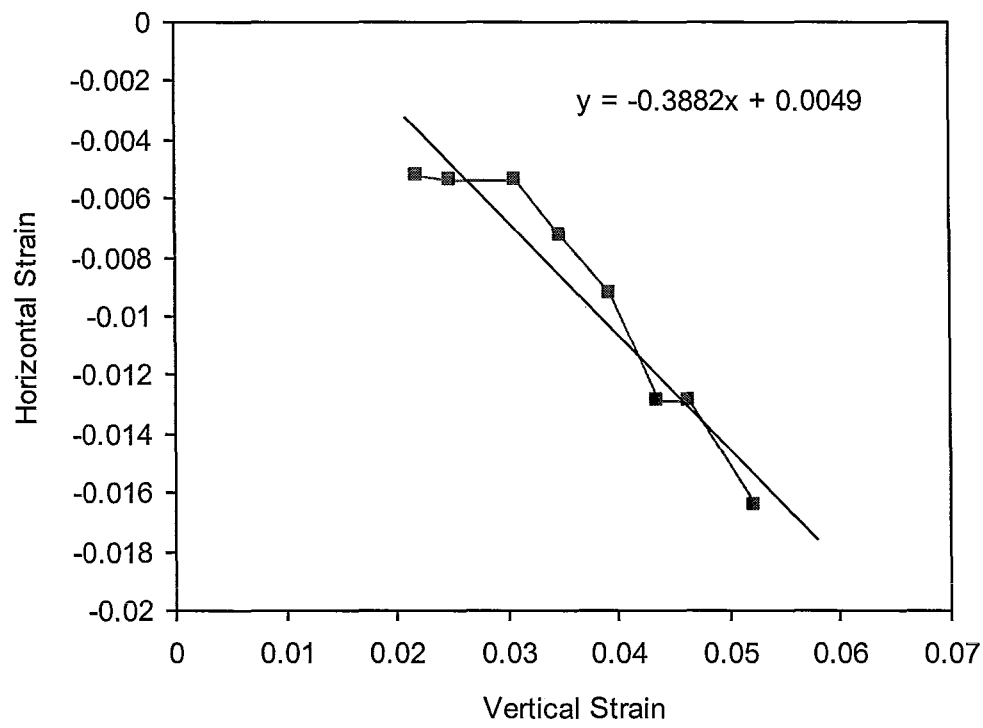

Fig. 3-6 Variation of (a) vertical stress and (b) horizontal strain with vertical stress for kaolinite sample at the elastic range

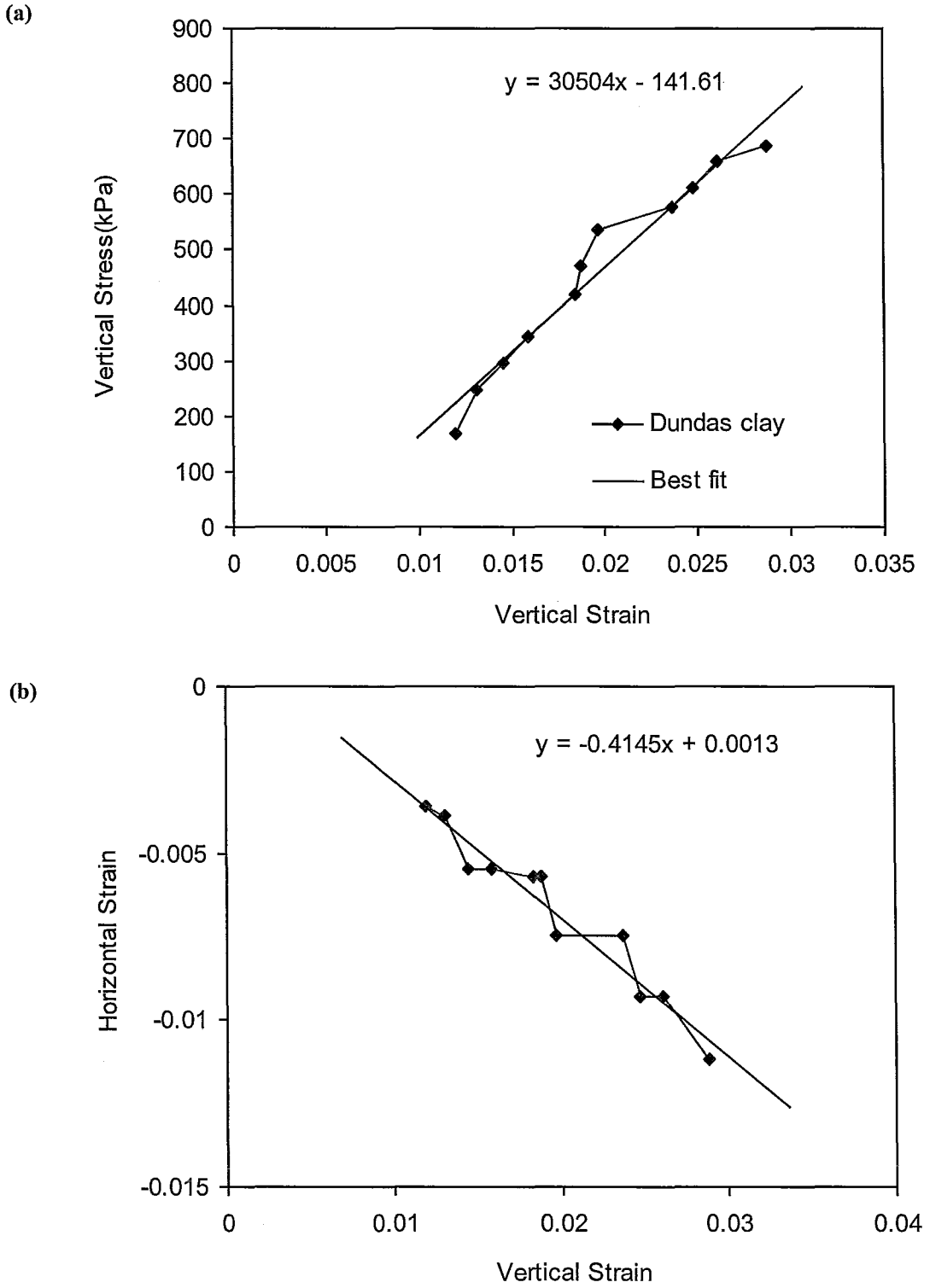

Fig. 3-7 Variation of (a) vertical stress and (b) horizontal strain with vertical stress for Dundas clay sample at the elastic range

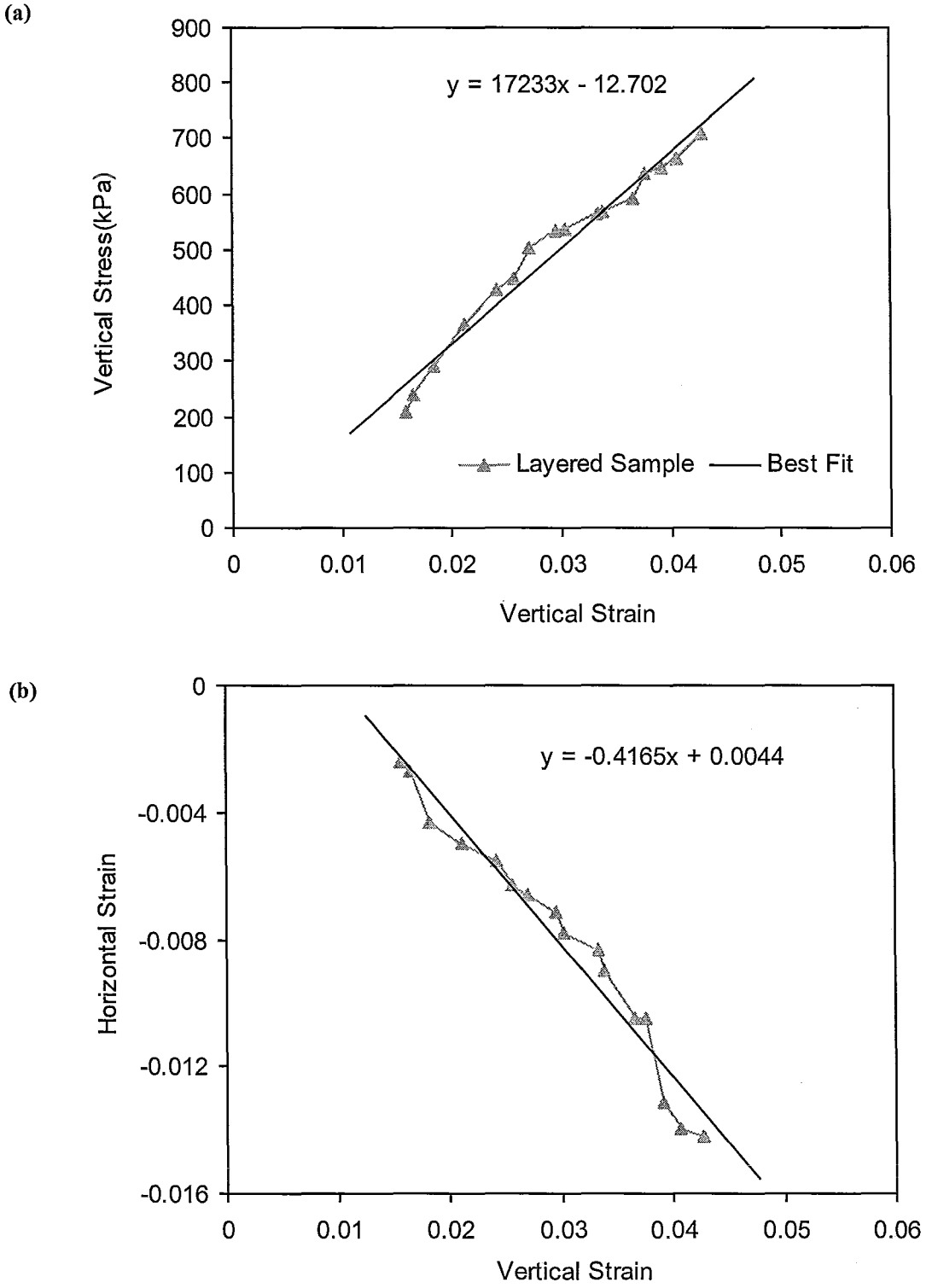

Fig. 3-8 Variation of (a) vertical stress and (b) horizontal strain with vertical stress for layers sample at the elastic range

To find the elastic constants the linear best fits were evaluated for each curve, with the slopes providing the elastic modulus and Poisson's ratio. The elastic modulus of the layered sample is between the elastic modulus of the constituent materials, as it was expected; i.e.

$$E_{kaolinite} = 15.25 \text{ MPa} \;\; ; \;\; \nu_{kaolinite} = 0.388$$
$$E_{Dundas\,caly} = 30.5 \text{ MPa} \;\; ; \;\; \nu_{Dundas\,caly} = 0.414$$
$$E_{Layered\,sample} = 17.23 \text{ MPa} \;\; ; \;\; \nu_{Layered\,sample} = 0.417$$

The general failure trend observed after each test was shear cracking in the samples as shown in Fig. 3-9 for the Dundas clay sample.

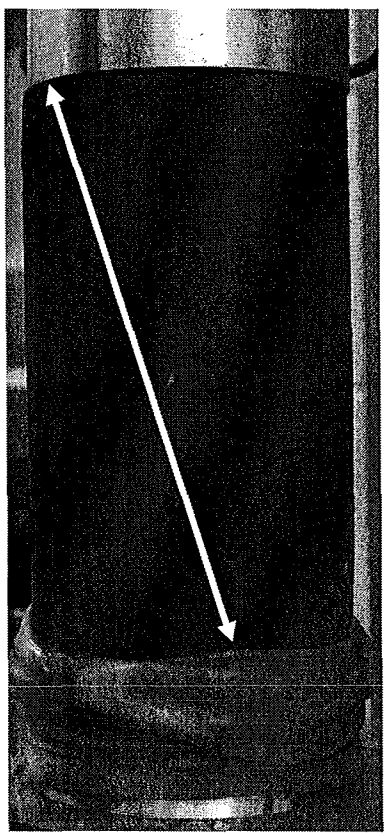

Fig. 3-9 Failure mechanism for Dundas clay sample in a triaxial compression test

3.5 Phase II

After having identified the elastic range of the samples, in Phase II of the experimental program the samples were tested only for that range. The experiments in Phase II focused on determining the elastic constants.

3.5.1 Test Specimens

The sample preparation method was the same as for Phase I, with the exception being that samples were also prepared in 12 layers (6 layers of Dundas clay and 6 layers of kaolinite) as shown in Fig. 3-10. These samples are referred to as Sample B type.

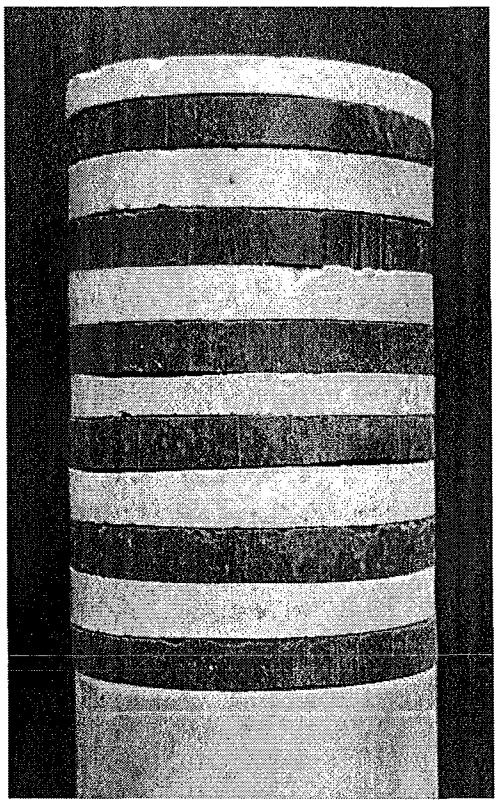

Fig. 3-10 Layered specimens investigated in phase two; consisting 6 layers of Dundas clay and 6 layers of kaolinite; Sample B (7cm in diameter and 10 cm high)

3.5.2 Test Setup

Samples were tested in a triaxial apparatus, however to find the elastic properties they were tested under both cyclic axial and lateral loading. Based on the results of Phase I, the stress level was selected so that the samples remained in the elastic range. To have a better control of applied confining pressure, the triaxial chamber was filled with water and the confining pressure was applied to the sample by controlling the water pressure, rather than by air. To minimize the effects of sample preparation flaws, e.g. the small gaps between the layers in Fig. 3-10, the samples were kept under the hydrostatic pressure for a duration of two days. This also helps to eliminate the unrepresentative stress-strain behavior observed at the first stage of the tests in Fig. 3-5.

Keeping the stress level at the elastic range enabled the samples to be reused for more than one loading path. This helped save time and lead to more consistent results, since making identical samples would have been exceptionally difficult. Fig. 3-11 and 3-12 show a schematic and actual test setup used for this phase of the study, respectively.

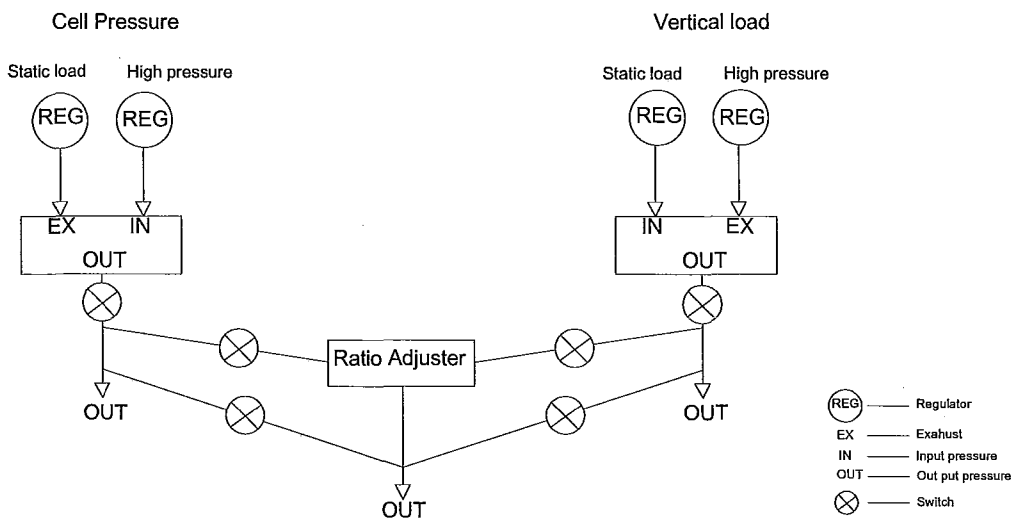

Fig. 3-11 Schematic of the test setup used in phase two, stress path setup

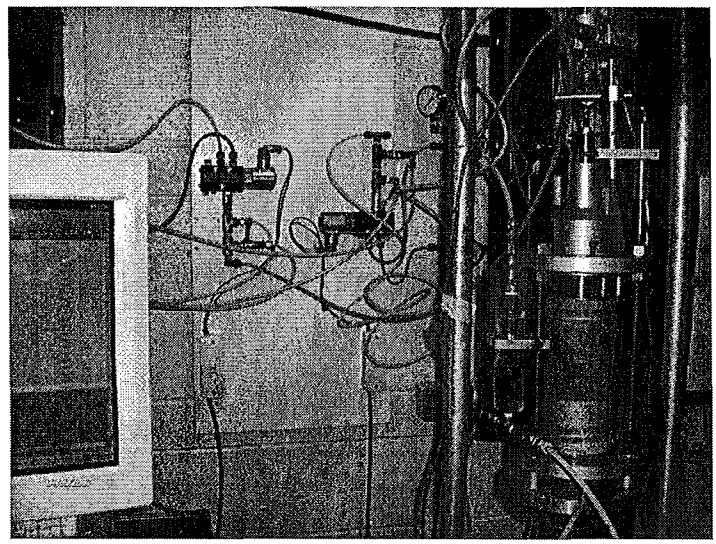

Fig. 3-12 Test setup used in phase two, stress path setup

3.5.3 Experimental Results

In the first family of the tests, a triaxial sample of the Sample A type, was tested under a cyclical axial load. The confining pressure was kept constant throughout the experiment at $\sigma_3 = 48\,\text{kPa}$. During the first stage the load was applied as a square wave varying from $\sigma_1 = 160\,\text{kPa}$ to $\sigma_1 = 200\,\text{kPa}$ for 5 cycles as shown in Fig. 3-13.

The averaged states of vertical stress and vertical stress at the extremums of the applied load are shown in Fig. 3-14a. For the next stage of the test, the magnitude of the cyclic vertical load on the sample was varied from $\sigma_1 = 200\,\text{kPa}$ to $\sigma_1 = 240\,\text{kPa}$, again for 5 cycles and in a square wave form. The same procedure was followed for the last stage but with the loading interval of $\sigma_1 = 240\,\text{kPa}$ to $\sigma_1 = 253\,\text{kPa}$. Mohr circle representation of the testing procedure is presented in Fig. 3-15. The vertical displacement of the sample and the average change in the radius of central layers at each stress level are listed in Table 3-1. Note that the initial height of the sample was 10.1 cm.

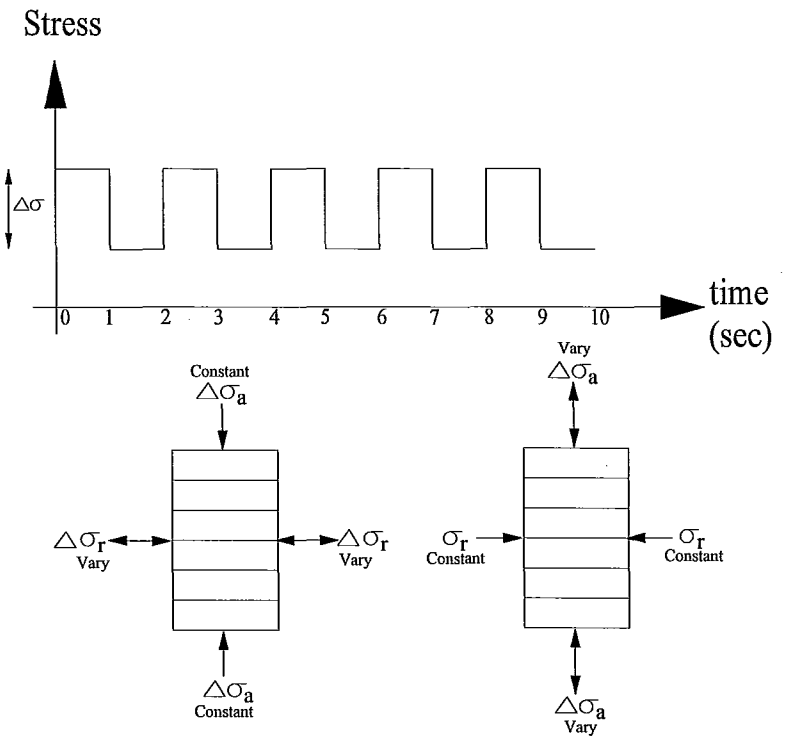

Fig. 3-13 Loading process in phase two, stress path loading pattern

A linear trend was observed in the stress-strain behavior as was expected. To find the elastic constants the lines of best fit were determined as shown in Fig. 3-14.

The same Sample A was then tested under cyclic lateral load, while keeping the vertical stress constant equal to 150 kPa. The loading intervals were chosen to be $\sigma_3 = 48-150\,\text{kPa}$, $\sigma_3 = 150-250\,\text{kPa}$ and $\sigma_3 = 250-350\,\text{kPa}$, with 5 cycles for each interval. The Mohr circle representation of the testing procedure is presented in Fig. 3-16, and the test results, in the form of averaged states of lateral stress and axial/lateral strain at the load extremums, are presented in Fig. 3-17. The vertical displacement of the sample and the average change in the radius of central layers at each stress level are listed in Table 3-2. Once again a linear pattern was observed in the stress-strain behavior. The linear best fits were used in the identification of elastic characteristics.

Table 3-1 Results of triaxial test with cyclic axial load on Sample A; the vertical displacement of the sample and the average change in the radius of central layers at different stress levels

Vertical Stress (kPa)	200	240	253
Vertical Displacement (mm)	-0.234078	-0.504847	-0.573579
Change in Radius (mm)	0.028	0.0525	0.0637

(a)

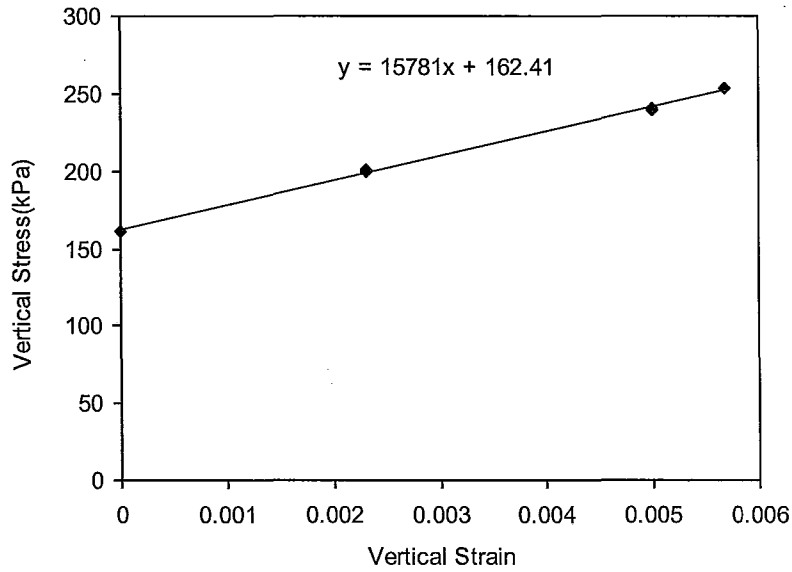

(b)

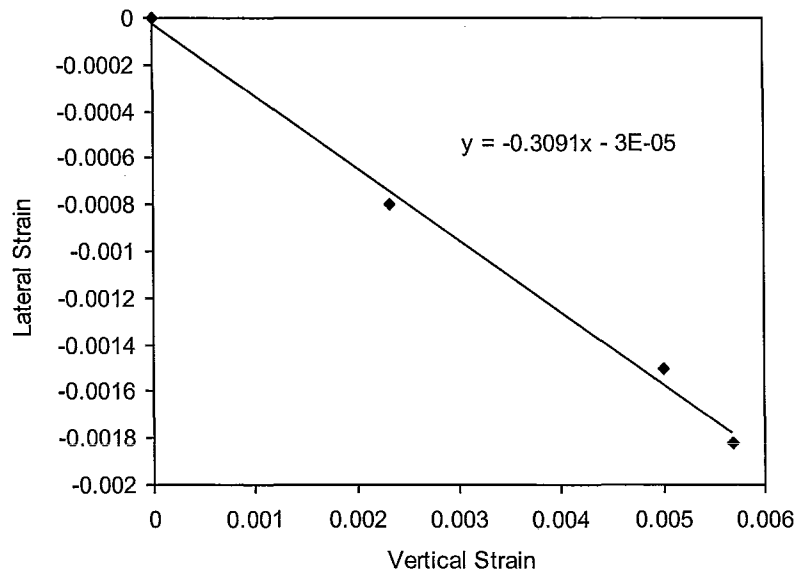

Fig. 3-14 Results of triaxial test with cyclic axial load on Sample A; (a) averaged states of vertical stress and vertical strain at the load extremums and the best fit to the experimental data and (b) variation of lateral strain versus vertical strain and the linear best fit

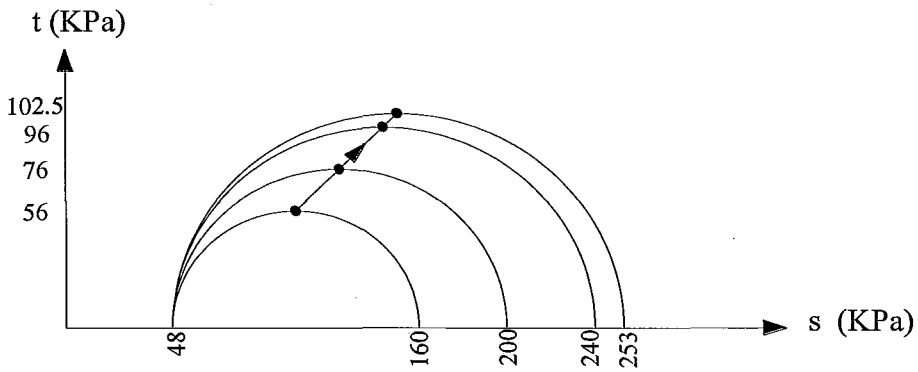

Fig. 3-15 Mohr circle representation of a triaxial test with cyclic axial load;

$$s = (\sigma_v + \sigma_h)/2 \quad , \quad t = (\sigma_v - \sigma h)/2$$

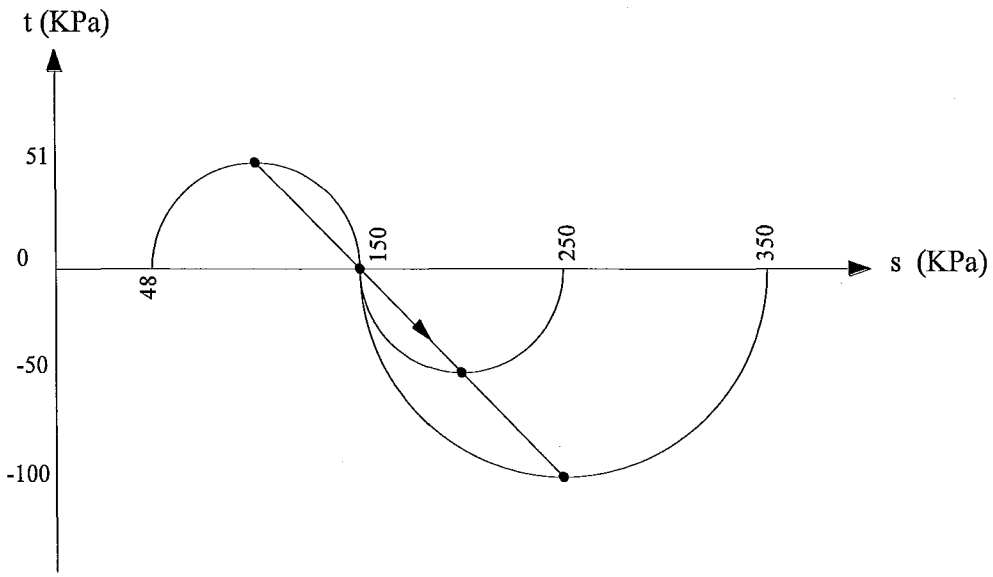

Fig. 3-16 Mohr circle representation of a triaxial test with cyclic lateral load

Table 3-2 Results of triaxial test with cyclic lateral load on Sample A; the vertical displacement of the sample and the average change in the radius of central layers at different stress levels

Horizontal Stress (kPa)	150	250	300
Vertical Displacement (mm)	0.454512	0.979731	1.11154
Change in Radius (mm)	-0.136	-0.243	-0.2865

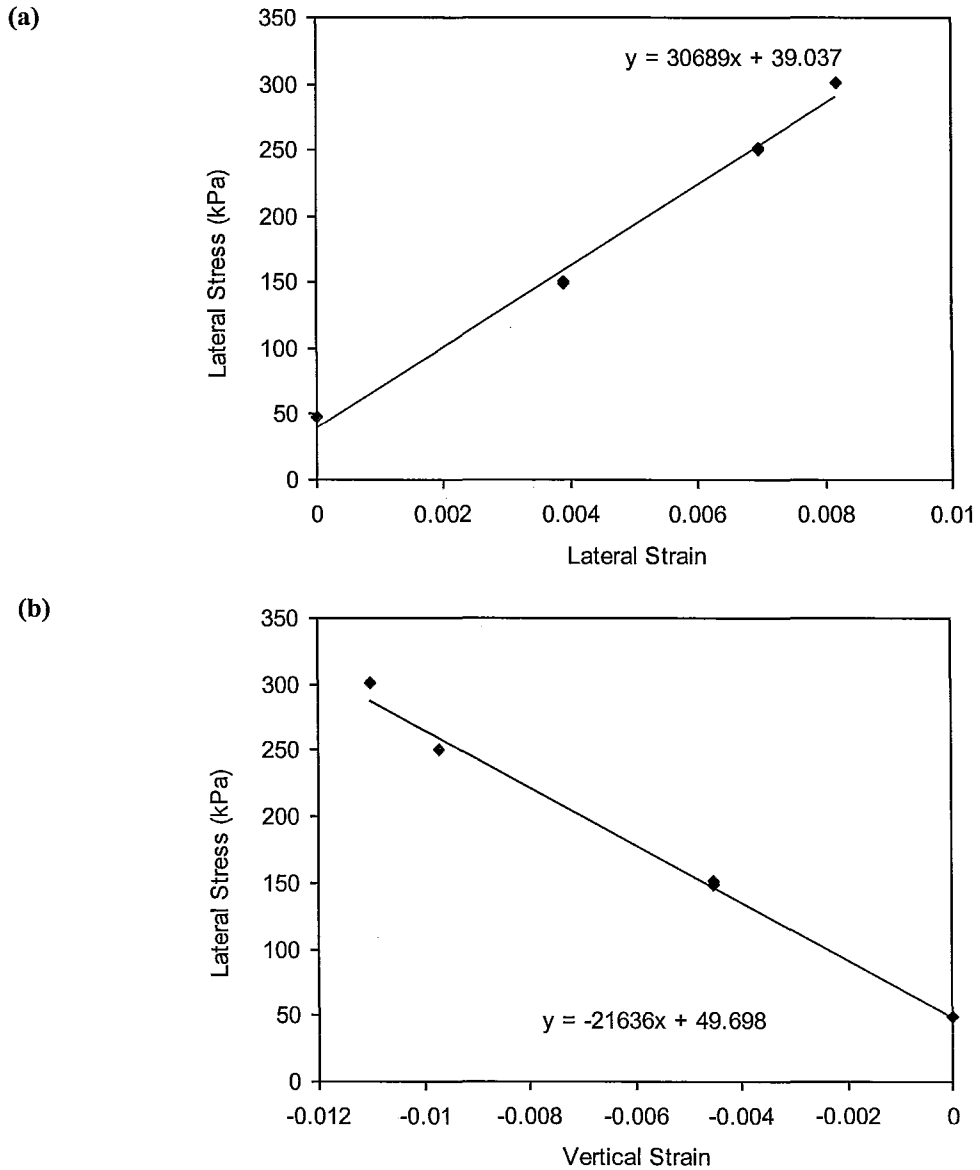

Fig. 3-17 Results of triaxial test with cyclic lateral load on Sample A; (a) averaged states of lateral stress and lateral strain at the load extremums and the best fit to the data ; (b) averaged states of lateral stress and vertical strain at the load extremums and the best fit to the data

For the second family of tests a triaxial sample of Sample B type was tested under a cyclic axial load. Analogous to the previous tests, the confining pressure was kept constant at $\sigma_3 = 48\,\text{kPa}$. In the first stage the load was applied in a square wave form varying from $\sigma_1 = 154\,\text{kPa}$ to $\sigma_1 = 192\,\text{kPa}$ for 5 cycles. The cyclic axial load intervals for the next stages of the test were $\sigma_1 = 192-230\,\text{kPa}$ and $\sigma_1 = 230-242\,\text{kPa}$, respectively. Table 3-3 presents the displacement of the sample and the average change in the radius of central layers at each stress level.

As illustrated in Fig. 3-18a, a linear trend was observed in the stress-strain behavior. The linear best fit to the experimental data in Fig. 3-18a and Fig. 3-18b was used to identify the elastic properties of the sample.

The same sample was also tested under cyclic lateral load, with constant vertical stress of $\sigma_1 = 150\,\text{kPa}$. The loading intervals were chosen to be $\sigma_3 = 49-150\,\text{kPa}$, $\sigma_3 = 150-250\,\text{kPa}$ and $\sigma_3 = 250-300\,\text{kPa}$, with 5 cycles for each interval. Table 3-4 presents the displacements of the sample at each stress level. The test results, in the form of averaged states of lateral stress and axial/lateral strain at the load extremums, are presented in Fig. 3-19. The linear pattern that was observed in the first two intervals was selected to find the linear best fits in Fig. 3-19a and Fig. 3-19b. Sample B tested here was 10.3 high.

Table 3-3 Results of triaxial test with cyclic axial load on sample B; the vertical displacement of the sample and the average change in the radius of central layers at different stress levels

Vertical Stress (kPa)	192	230	242
Vertical Displacement (mm)	-0.229315	-0.477598	-0.551666
Change in Radius (mm)	0.028	0.063	0.0705

(a)

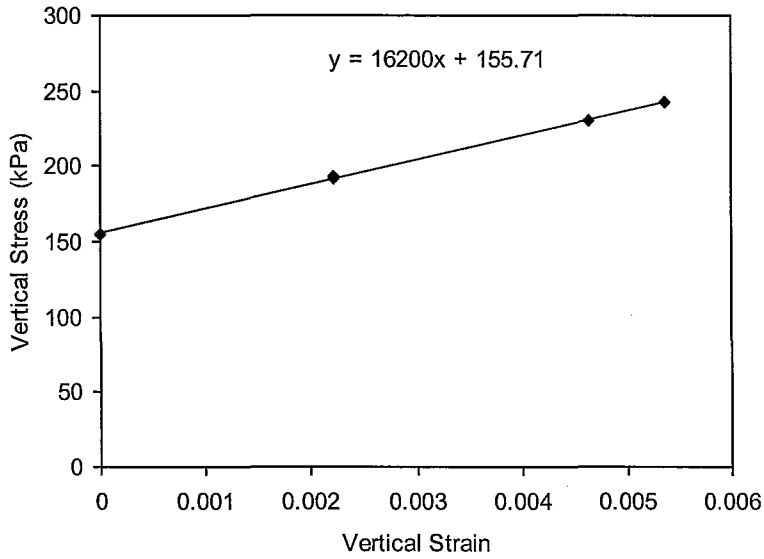

(b)

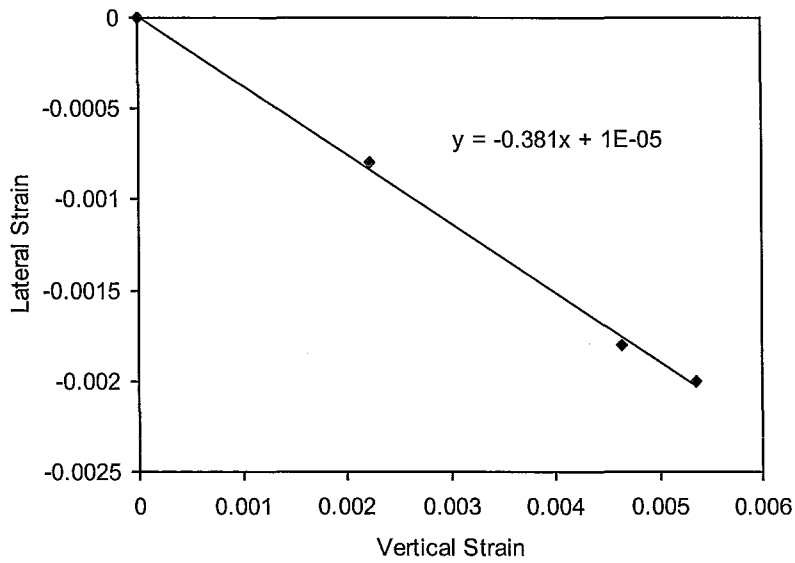

Fig. 3-18 Results of triaxial test with cyclic axial load on sample B; (a) averaged states of vertical stress and vertical strain at the load extremums and the best fit to the experimental data and (b) variation of lateral strain versus vertical strain and the linear best fit

Table 3-4 Results of triaxial test with cyclic lateral load on sample B; the vertical displacement of the sample and the average change in the radius of central layers at different stress levels

Lateral Stress (kPa)	150	250	300
Vertical Displacement (mm)	0.498521	0.824425	0.8755172
Change in Radius (mm)	-0.113	-0.215	-0.23

(a)

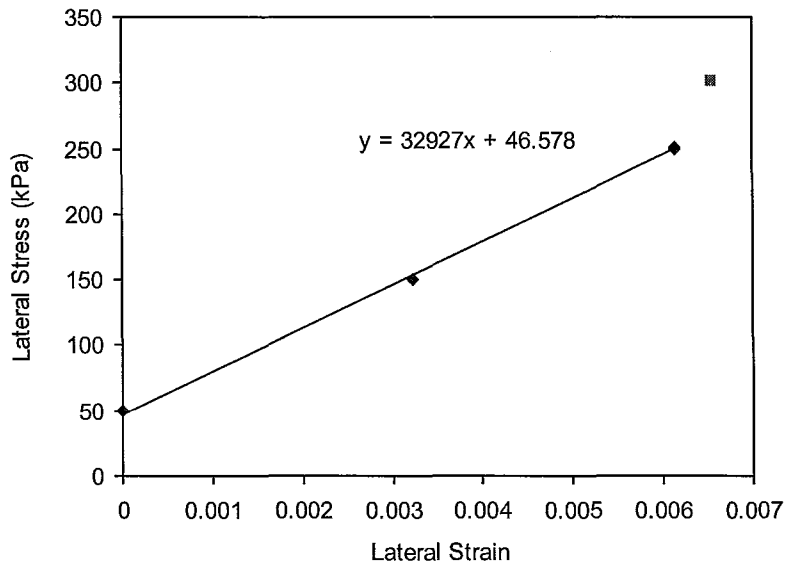

(b)

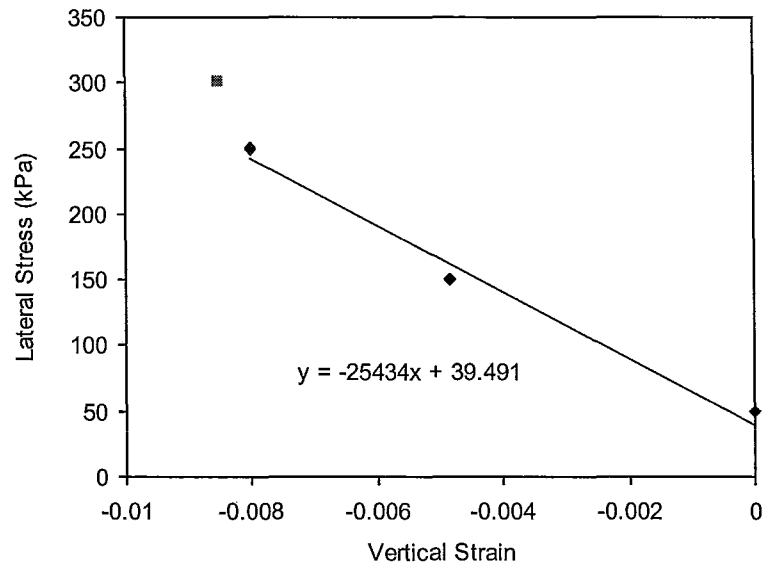

Fig. 3-19 Results of triaxial test with cyclic lateral load on sample B; (a) averaged states of lateral stress and lateral strain at the load extremums and the best fit to the data ; (b) averaged states of lateral stress and vertical strain at the load extremums and the best fit to the data

The properties of the homogeneous samples, i.e. Dundas clay and kaolinite, were tested in similar manner using the same stress path and loading sequences. The results of triaxial tests with cyclic axial load on a sample of Dundas clay are presented in Fig. 3-20. The prepared Dundas clay sample was 10.9 cm high. The cyclic axial load intervals were $\sigma_1 = 148 - 215\,\text{kPa}$, $\sigma_1 = 215 - 240\,\text{kPa}$ and $\sigma_1 = 240 - 255\,\text{kPa}$. The linear best fit to the obtained data is presented in Fig. 3-20a and Fig. 3-20b and could be used to identify the elastic properties of Dundas clay.

The behavior of Dundas clay in triaxial test with cyclic lateral load, under a constant vertical stress, is presented in Fig. 3-21. The loading intervals were chosen to be $\sigma_3 = 49 - 150\,\text{kPa}$, $\sigma_3 = 150 - 250\,\text{kPa}$ and $\sigma_3 = 250 - 300\,\text{kPa}$. The linear best fits are presented in Fig. 3-21b and Fig. 3-21b. Fig. 3-22 and Fig. 3-23 present the results of similar tests on kaolinite. The koalinite sample was 11.3 cm high.

As mentioned earlier, the experimental results presented in this chapter investigated the elastic properties of layered system to confirm the concept of "equivalent" transversely isotropic material. The data analysis of the results and identification of material properties is presented in the following chapter.

Table 3-5 Results of triaxial test with cyclic axial load on Dundas clay; the vertical displacement of the sample and the average change in the radius of central layers at different stress levels

Vertical Stress (kPa)	215	240	255
Vertical Displacement (mm)	-0.301555	-0.378797	-0.412715
Change in Radius (mm)	0.0322	0.0438	0.0462

(a)

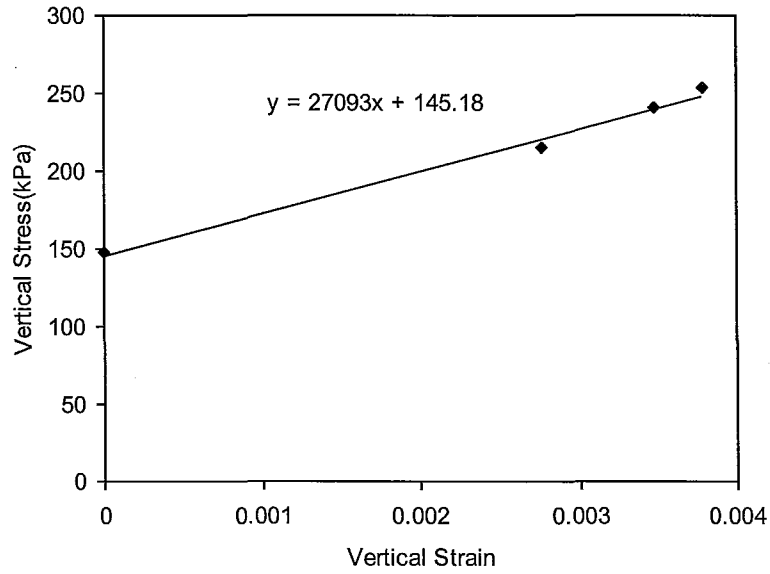

(b)

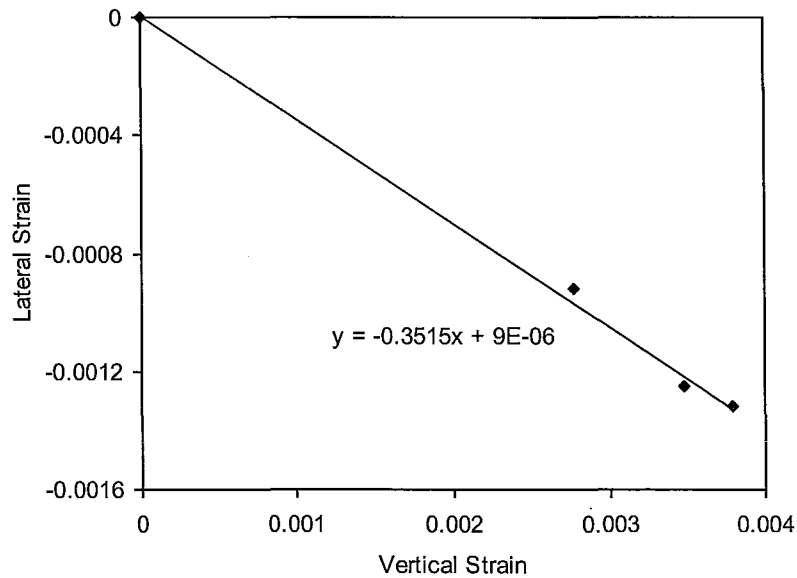

Fig. 3-20 Results of triaxial test with cyclic axial load on Dundas clay; (a) averaged states of vertical stress and vertical strain at the load extremums and the best fit to the experimental data and (b) variation of lateral strain versus vertical strain and the linear best fit

Table 3-6 Results of triaxial test with cyclic lateral load on Dundas clay; the vertical displacement of the sample and the average change in the radius of central layers at different stress levels

Vertical Stress (kPa)	150	250	300
Vertical Displacement (mm)	0.190751	0.545341	0.654261
Change in Radius (mm)	-0.0324	-0.156	-0.1729

(a)

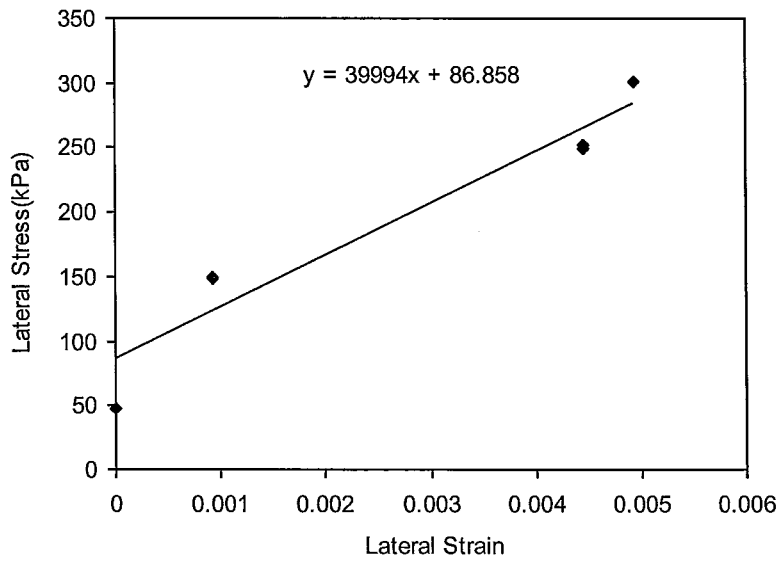

(b)

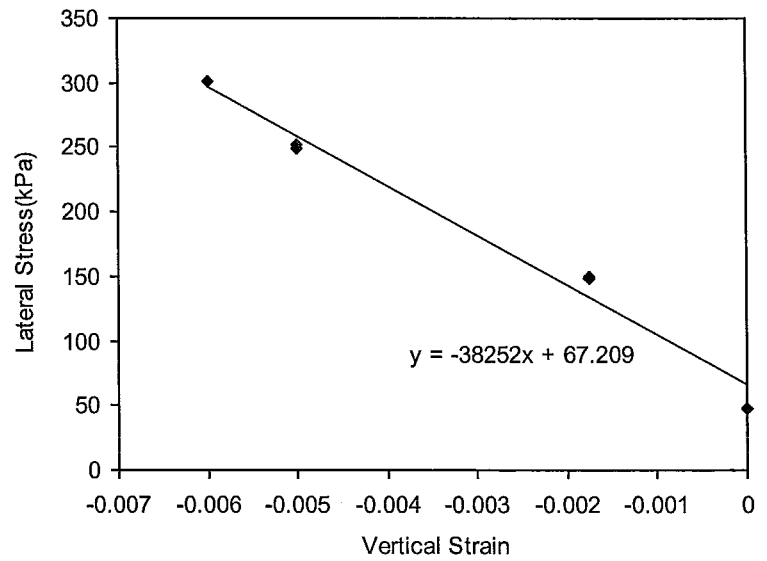

Fig. 3-21 Results of triaxial test with cyclic lateral load on Dundas clay; (a) averaged states of lateral stress and lateral strain at the load extremums and the best fit to the data ; (b) averaged states of lateral stress and vertical strain at the load extremums and the best fit to the data

Table 3-7 Results of triaxial test with cyclic axial load on kaolinite; the vertical displacement of the sample and the average change in the radius of central layers at different stress levels

Vertical Stress (kPa)	215	241	255
Vertical Displacement (mm)	-0.555988	-1.002792	-1.127560
Change in Radius (mm)	0.0666	0.1172	0.1406

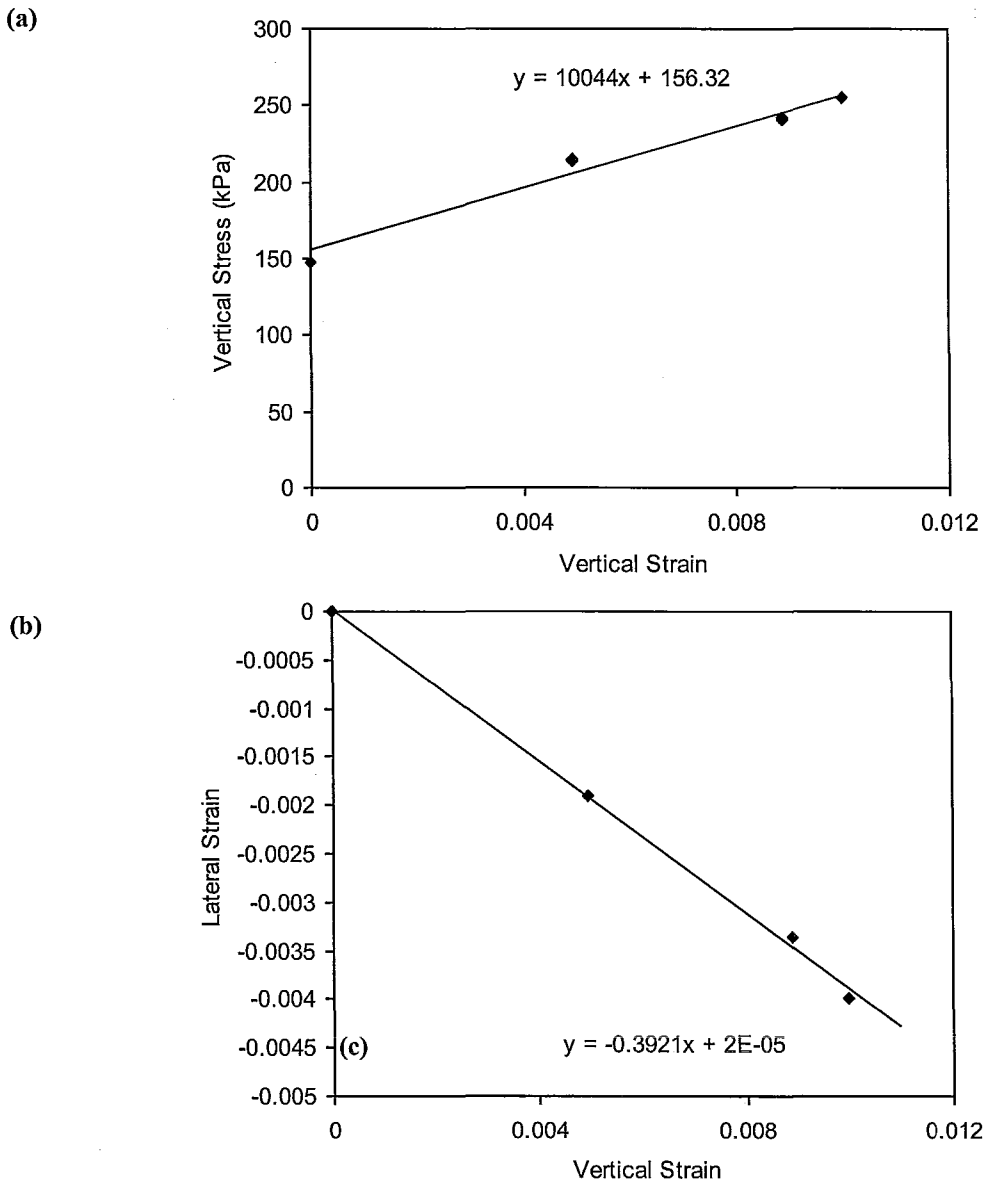

Fig. 3-22 Results of triaxial test with cyclic axial load on kaolinite; (a) averaged states of vertical stress and vertical strain at the load extremums and the best fit to the experimental data and (b) variation of lateral strain versus vertical strain and the linear best fit

Table 3-8 Results of triaxial test with cyclic lateral load on kaolinite; the vertical displacement of the sample and the average change in the radius of central layers at different stress levels

Vertical Stress (kPa)	150	250	300
Vertical Displacement (mm)	0.757118	1.864538	2.147421
Change in Radius (mm)	-0.1112	-0.347	-0.4503

(a)

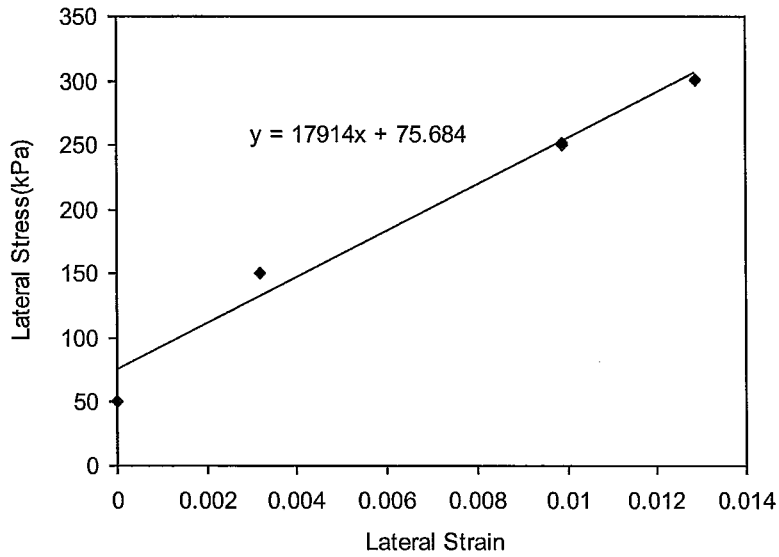

(b)

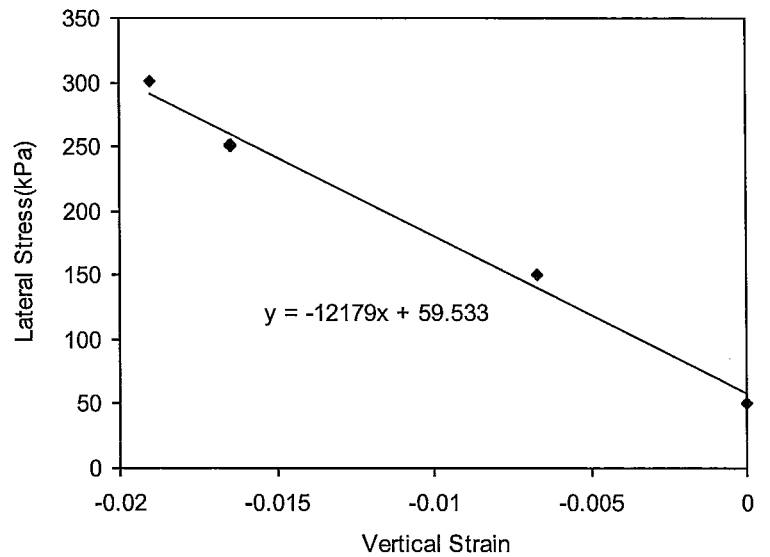

Fig. 3-23 Results of triaxial test with cyclic lateral load on kaolinite; (a) averaged states of lateral stress and lateral strain at the load extremums and the best fit to the data ; (b) averaged states of lateral stress and vertical strain at the load extremums and the best fit to the data

CHAPTER 4
ANALYSIS AND VERIFICATION

4.1 Introduction

The experimental data obtained in the previous chapter is analyzed next, with the elastic properties of Dundas clay and kaolinite and the layered samples made of these materials being identified. The material properties of the layered material, i.e. the "equivalent" transversely isotropic material, are obtained from the experiments conducted on Samples A and B and a comparison is made between the measured and calculated material properties of the "equivalent" transversely isotropic material. Finite element simulations of the tests were carried out to further investigate the behavior the equivalent material with the FE results being compared to the results obtained from the mathematical formulation and experiments.

4.2 Elastic Characteristics of the Equivalent Transversely Isotropic Material

In this section, the elastic constants of the equivalent transversely isotropic material (Samples A and B) are identified. The following subsection identifies the elastic constants from the experimental test data. In the subsequent subsection, the elastic constants of the equivalent transversely isotropic samples are estimated based on the equations presented in Chapter 2 together with the properties of constituent materials identified from the experiments.

4.2.1 Properties of the Layered Samples of Types A and B

To find the properties of the equivalent transversely isotropic material, first the properties of the constituents must be identified.

It should be noted that only normal components of stress and strain were involved in the experiments presented in Chapter 3. For an isotropic material, such as Dundas clay and kaolinite, the elastic constitutive relation can be simplified to

$$\begin{Bmatrix} \dot{\varepsilon}_{11} \\ \dot{\varepsilon}_{22} \\ \dot{\varepsilon}_{33} \end{Bmatrix} = \begin{bmatrix} \frac{1}{E} & \frac{-\nu}{E} & \frac{-\nu}{E} \\ & \frac{1}{E} & \frac{-\nu}{E} \\ Sym. & & \frac{1}{E} \end{bmatrix} \begin{Bmatrix} \dot{\sigma}_{11} \\ \dot{\sigma}_{22} \\ \dot{\sigma}_{33} \end{Bmatrix} \tag{4.1}$$

Note that in the triaxial tests with cyclic axial load the stress rates were such that $\dot{\sigma}_{11} = \dot{\sigma}_{22} = 0$ and $\dot{\sigma}_{33} \neq 0$. Strain state was such that the lateral strains were equal, i.e. $\dot{\varepsilon}_{11} = \dot{\varepsilon}_{22}$. Considering the loading conditions in the cyclic axial and cyclic lateral triaxial tests with the results presented in Fig 3-20 and Fig 3-21 on Dundas clay, one can obtain using Eqn. (4.1): $E = 27.09$ MPa, $\nu = 0.352$, $E/(2\nu) = 38.25$ MPa and $E/(1-\nu) = 39.99$ MPa. The results for the cyclic lateral triaxial test can be reinterpreted as $E = 26.26$ MPa, $\nu = 0.343$. Averaging the obtained values of the elastic constants for Dundas clay leads to

$$\begin{aligned} E_{Dundas\ clay} &= 26.68 \text{ MPa} \ ; \ \nu_{Dundas\ clay} = 0.348 \\ \lambda_{Dundas\ clay} &= 22.66 \text{ MPa} \ ; \ \mu_{Dundas\ clay} = 9.9 \text{ MPa} \end{aligned} \tag{4.2}$$

With the same argument for the results presented in Fig 3-22 and Fig 3-23 for kaolinite under cyclic axial load, it can be concluded that $E = 10.04$ MPa, $\nu = 0.392$, and $E/(2\nu) = 12.18$ MPa, $E/(1-\nu) = 17.91$ MPa. The results for the cyclic lateral tests can be expressed as $E = 10.32$ MPa, $\nu = 0.424$, thus by averaging one finds

$$E_{kaolinite} = 10.18 \text{ MPa} \;;\; \nu_{kaolinite} = 0.408$$
$$\lambda_{kaolinite} = 16.03 \text{ MPa} \;;\; \mu_{kaolinite} = 3.615 \text{ MPa} \tag{4.3}$$

Considering only normal components of the stress and strain, for an elastic transversely isotropic material the elastic stress-strain relationship can be simplified as (also see Eqn. (2.36))

$$\begin{Bmatrix} \dot{\varepsilon}_{11} \\ \dot{\varepsilon}_{22} \\ \dot{\varepsilon}_{33} \end{Bmatrix} = \begin{bmatrix} \frac{1}{E_h} & \frac{-\nu_h}{E_h} & \frac{-\nu_{vh}}{E_v} \\ & \frac{1}{E_h} & \frac{-\nu_{vh}}{E_v} \\ Sym. & & \frac{1}{E_v} \end{bmatrix} \begin{Bmatrix} \dot{\sigma}_{11} \\ \dot{\sigma}_{22} \\ \dot{\sigma}_{33} \end{Bmatrix} \tag{4.4}$$

The symmetry of rotation is around the vertical axis (v) or direction 3 and plane of isotropy is horizontal (h) parallel to the plane 1-2. The dot above the stresses and strains should be interpreted as change in stress and strain.

The results presented in Fig 3-14, 17, 18 and 19, were obtained from triaxial tests with cyclic vertical load on Samples A and B, respectively, such that $\dot{\sigma}_{11} = \dot{\sigma}_{22} = 0$. Thus

the only non-zero component of stress tensor was $\dot{\sigma}_{33}$. The strain state was such that the lateral strains were equal, i.e. $\dot{\varepsilon}_{11} = \dot{\varepsilon}_{22}$. Considering the pair $(\dot{\varepsilon}_{33}, \dot{\sigma}_{33})$ in Eqn. (4.4) and the linear best fit from Fig 3-14a it can be shown that $E_v = 15.78$ MPa. Also from Eqn. (4.4), and the linear best fit shown in Fig 3-14b one can find that $\nu_{vh} = 0.3091$. Based on similar arguments with respect to the results presented in Fig 3-18, another evaluation of the aforementioned parameters are $E_v = 16.2$ MPa and $\nu_{vh} = 0.381$.

At this point it is worth to recall that Sample A consists of alternates of 3 layers of Dundas clay and 3 layers of kaolinite while Sample B consists of 6 layers of each of the aforementioned homogeneous materials.

The results presented in Fig 3-17 and Fig 3-19, are from triaxial tests with cyclic lateral load with a constant vertical stress on Samples A and B, respectively. The loading condition is such that $\dot{\sigma}_{33} = 0$ and the other two components of stress tensor are equal and non-zero $\dot{\sigma}_{11} = \dot{\sigma}_{22} \neq 0$. Once again, the strain state is such that the lateral strains are equal; i.e. $\dot{\varepsilon}_{11} = \dot{\varepsilon}_{22}$. Considering the pair $(\dot{\varepsilon}_{11}, \dot{\sigma}_{11})$ or $(\dot{\varepsilon}_{22}, \dot{\sigma}_{22})$ in Eqn. (4.4) and the linear best fits in Fig 3-17a it can be concluded that $E_h/(1-\nu_h) = 30.69$ MPa. Also from the linear best fit shown in Fig 3-17b there is $E_v/(2\nu_{vh}) = 21.64$ MPa. From Fig 3-19, another evaluation of the abovementioned terms are $E_h/(1-\nu_h) = 32.93$ MPa and $E_v/(2\nu_{vh}) = 25.43$ MPa.

In view of Eqn. (2.48) one can conclude that the Samples A and B should have the same elastic constants, since for Sample A and B there is $d_{1A} = d_{2A} = 2d_{1B} = 2d_{2B}$.

From the discussion presented and conclusions derived on the experimental results obtained for Samples A and B, the averaged elastic constants of the equivalent transversely isotropic material from both samples yield

$$\left.\begin{aligned} &\text{A: } \nu_{vh} = 0.3091 \\ &\text{B: } \nu_{vh} = 0.3810 \end{aligned}\right\} \Rightarrow \nu_{vh} = 0.345$$

$$\left.\begin{aligned} &\text{A: } E_v = 15.78 \text{ MPa} \ , \ E_v/(2\nu_{vh}) = 21.64 \text{ MPa} \\ &\text{B: } E_v = 16.20 \text{ MPa} \ , \ E_v/(2\nu_{vh}) = 25.43 \text{ MPa} \end{aligned}\right\} \Rightarrow E_v = 16.12 \text{ MPa} \qquad (4.5)$$

$$\left.\begin{aligned} &\text{A: } E_h/(1-\nu_h) = 30.69 \text{ MPa} \\ &\text{B: } E_h/(1-\nu_h) = 32.93 \text{ MPa} \\ &\text{assuming} \quad \nu_h = 0.375 \end{aligned}\right\} \Rightarrow E_h = 19.88 \text{ MPa}$$

It should be noted that some of the difference in the elastic properties of Samples A and B may be due to differences in stress and strain fields. It is most likely that the differences are associated with the sample fabrication; i.e. the samples were not perfect.

4.2.2 Properties of the Equivalent Transversely Isotropic Material, Samples A and B

Referring to Eqn. (2.48) the components of the elastic constitutive tensor can be identified from the values presented in Eqns. (4.2) and (4.3)

$$\begin{aligned} D_{1111} &= D_{1111} = 32.53 \text{ MPa} \\ D_{3333} &= 30.06 \text{ MPa} \\ D_{1122} &= 19.01 \text{ MPa} \\ D_{1133} &= D_{2233} = 18.38 \text{ MPa} \end{aligned} \qquad (4.6)$$

By considering the values determined and Eqns. (2.36) and (2.37) with some mathematical manipulation one can obtain

$$\begin{aligned} E_h &= 18.45 \text{ MPa} \;\; ; \;\; \nu_h = 0.365 \\ E_v &= 16.95 \text{ MPa} \;\; ; \;\; \nu_{vh} = 0.357 \end{aligned} \tag{4.7}$$

The results on the elastic constants from the formulation (Eqn. (4.7)) and from the experiments (Eqn. (4.5)) are in a good agreement, with a relative error of less than 10%.

$$\begin{aligned} &\text{Experiments} \quad E_h = 19.88 \text{ MPa} \;\; , \;\; E_v = 16.12 \text{ MPa} \;\; , \;\; \nu_{vh} = 0.345 \\ &\text{Fomulation} \quad E_h = 18.45 \text{ MPa} \;\; , \;\; E_v = 16.95 \text{ MPa} \;\; , \;\; \nu_{vh} = 0.357 \end{aligned} \tag{4.8}$$

4.3 Equivalent Transversely Isotropic Material in FEM

In this section, the mechanical behavior of the layered material (Samples A and B) is analyzed via finite element simulations. The finite element package used here is ABAQUS. The elastic properties of Dundas clay and kaolinite layers are depicted from the values presented in Eqns. (4.2) and (4.3), respectively. The averaged stress-deformation characteristics from the simulations are then compared to the experimental results. The geometry and finite element meshes of the Samples A and B are illustrated in Fig. 4-1. The dimensions of the samples are the same as reported in Chapter 3. The samples were simulated using an axial symmetric condition. To include the effects of loading platen on the top of the samples, a rigid block was placed on top of the sample and the vertical pressure was applied on top of that block. The contact surface between the platen and the sample was considered to be frictionless. Roller boundary condition was considered along the bottom edge of the model.

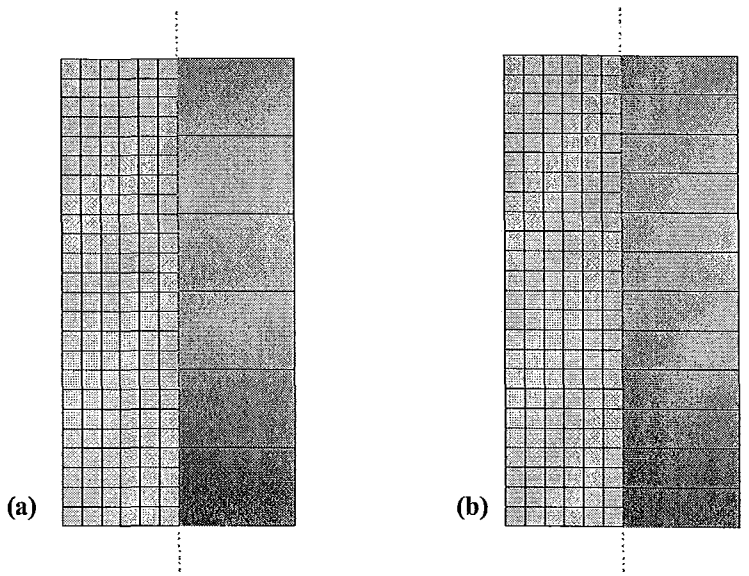

Fig. 4-1 Geometry and the Finite elememt mesh of the models of (a) Sample A and (b) Sample B

The loading steps in the simulations follow the same procedures as in the experiments.

In the first simulation on Sample A, an initial vertical pressure of 160 kPa and lateral pressure of 50 kPa were applied to the models to create similar initial condition (see Table 3-1, Fig. 3-14). In the second step of loading for the axial compression test on Sample A, analogous to the loading steps presented in Table 3-1 and Fig. 3-14, the axial pressure on top of the sample was first increased to 200 kPa, then 240 kPa and finally 253 kPa. The vertical displacement and the average change in the radius of the sample at each stress level are listed in Table 3-1. The vertical and radial deformations of the sample are compared to the experimental values and the relative errors are presented in the same table. The comparison shows a reasonable agreement between the experimental and numerical results.

Table 4-1 Numerical and experimental results of axial compression test on Sample A; the vertical displacement of the sample and the average change in the radius of central layers at different stress levels, and the relative errors

Vertical Stress (kPa)		200	240	253
Vertical Displacement(mm)	Numerical	-0.252351	-0.504701	-0.586711
	Experimental	-0.234078	-0.504847	-0.573579
Relative Error (Vertical)		7.81%	0.03%	2.29%
Change in Radius (mm)	Numerical	0.03294681	0.06589358	0.07660135
	Experimental	0.028	0.0525	0.0637
Relative Error (Radial)		17.67%	25.51%	20.25%

The contours of vertical and horizontal stress in the deformed domain for simulation of Sample A are presented in Table 3-2. Note that the deformations are magnified by a factor of 5 to better illustrate the deformation pattern. The stress distribution, in general, is not uniform and although the applied loads on the sample are all compressive, the kaolinite layers are under tension in horizontal direction near the axis of symmetry of the sample. It should be kept in mind that the concept of equivalent transversely isotropic material is only investigated in elastic range in this study and therefore the consideration of such detail is secondary, as we are interested in average response. As mentioned in the first chapter, in a system consisting of layers of different materials, the weak layer often facilitates failure. The failure mechanism of such systems is beyond the scope of this research.

For lateral compression test on Sample A, at the first step of the loading a vertical stress of 150 kPa and a lateral stress of 50 kPa were applied to the sample, and at the second step the lateral pressure was increased to 150 kPa, 250 kPa and finally 300 kPa.

The results of the simulation are presented in Table 3-2. The simulation results are compared to the experimental values in Table 4-2 and the relative errors in the deformations are also presented. Clearly the numerical and experimental results are in a good agreement. The contours of vertical and horizontal stress in the deformed domain are shown in Fig. 4-3. Once again the stress distribution is not uniform.

Table 4-2 Numerical and experimental results of axial compression test on Sample A; the vertical displacement of the sample and the average change in the radius of central layers at different stress levels, and the relative errors

Horizontal Stress (kPa)		150	250	300
Vertical Displacement (mm)	Numerical	0.471118	0.942236	1.177796
	Experimental	0.454512	0.979731	1.11154
Relative Error (Vertical)		3.65%	3.83%	5.96%
Change in Radius (mm)	Numerical	-0.13131923	-0.26263839	-0.32829811
	Experimental	-0.136	-0.243	-0.2865
Relative Error (Lateral)		3.44%	8.08%	14.59%

Similar simulations were performed for Sample B. In the axial compression test the sample was first compressed under a vertical stress of 154 kPa and a radial stress of 50 kPa. At the second step the axial pressure was increased to 192 kPa, 230 kPa and finally 242 kPa. The results of the simulation are presented in Table 3-3. The simulation results are compared to the experimental values in Table 4-3 and the relative errors in the deformations are also presented. Clearly the numerical and experimental results are in a good agreement.

Table 4-3 Numerical and experimental results of axial compression test on Sample B; the vertical displacement of the sample and the average change in the radius of central layers at different stress levels, and the relative errors

Vertical Stress (kPa)		192	230	242
Vertical Displacement (mm)	Numerical	-0.231731	-0.462464	-0.536644
	Experimental	-0.229315	-0.477598	-0.551666
Relative Error (Vertical)		1.05%	3.17%	2.72%
Change in Radius (mm)	Numerical	0.0295044	0.059009	0.068326
	Experimental	0.028	0.063	0.0705
Relative Error (Lateral)		5.37%	6.34%	3.08%

For lateral compression test on Sample B, at the first step of the loading a vertical stress of 150 kPa and a lateral stress of 50 kPa were applied to the sample, and at the second step the lateral pressure was increased to 150 kPa, 250 kPa and finally 300 kPa. The results of the simulation are presented in Table 3-4. The simulation results are compared to the experimental values in Table 3-4 and the relative errors in the deformations are also presented. Except for the last increment, the numerical and experimental results are in a fair agreement.

The deformed mesh and contours of vertical and horizontal stress from the simulations on Sample B are presented in Fig. 4-4 and Fig. 4-5.

Comparing the results presented in Fig. 4-2 and Fig. 4-3 with the results in Fig. 4-4 and Fig. 4-5, one finds that the nonuniformity in the stress distribution has a similar pattern for Samples A and B, but the stress values are different. The fact that the stresses in 6 and 12 layer samples are different would indicate that some differences in the

evaluated elastic parameters should be expected. These differences are not captured in Eqn. (2.48). It should be noted that an increase in the number of layers for the given geometry appears to have the effect increasing the zones of uniform layer stresses; see, for example, Fig. 4-5 where the contour of vertical stress is more uniform along the left hand side when compared to that that shown in Fig. 4-3.

Table 4-4 Numerical and experimental results of lateral compression test on Sample B; the vertical displacement of the sample and the average change in the radius of central layers at different stress levels, and the relative errors

Lateral Stress (kPa)		150	250	300
Vertical Displacement (mm)	Numerical	0.444854	0.889709	1.112136
	Experimental	0.498521	0.824425	0.8755172
Relative Error (Vertical)		10.76%	7.92%	27.03%
Change in Radius (mm)	Numerical	-0.12542828	-0.25085656	-0.31357066
	Experimental	-0.113	-0.215	-0.23
Relative Error (Lateral)		11%	16.68%	36.33%

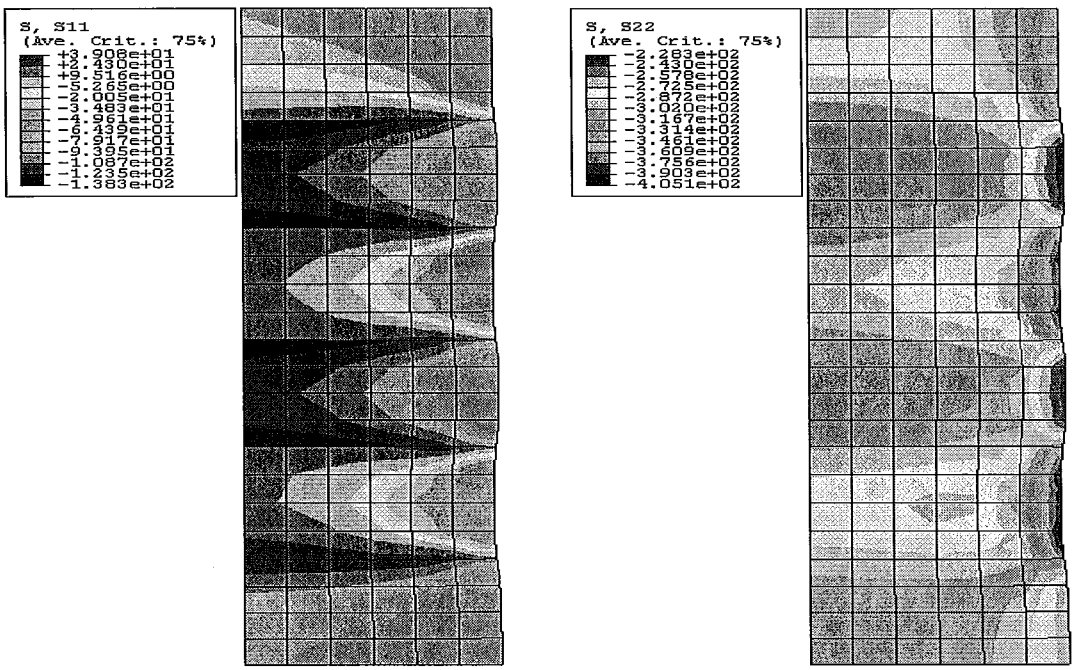

Fig. 4-2 FE simulation results on Sample A in an axial compression triaxial test; contours of vertical and horizontal stress in the deformed domain (deformation scale factor=5.0)

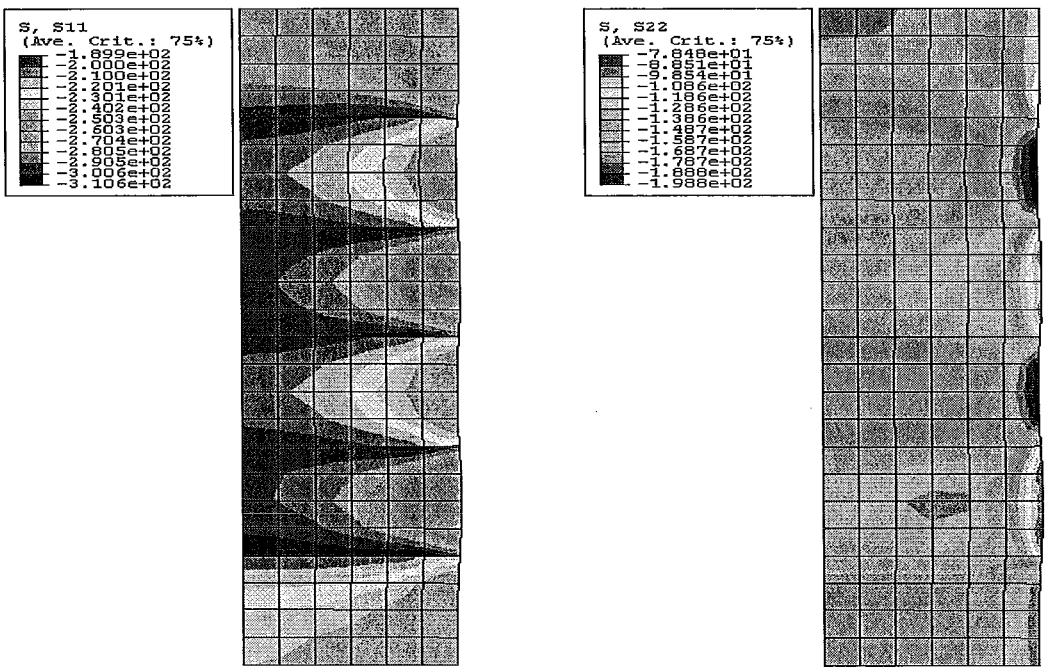

Fig. 4-3 FE simulation results on Sample A in a lateral compression triaxial test; contours of vertical and horizontal stress in the deformed domain (deformation scale factor=5.0)

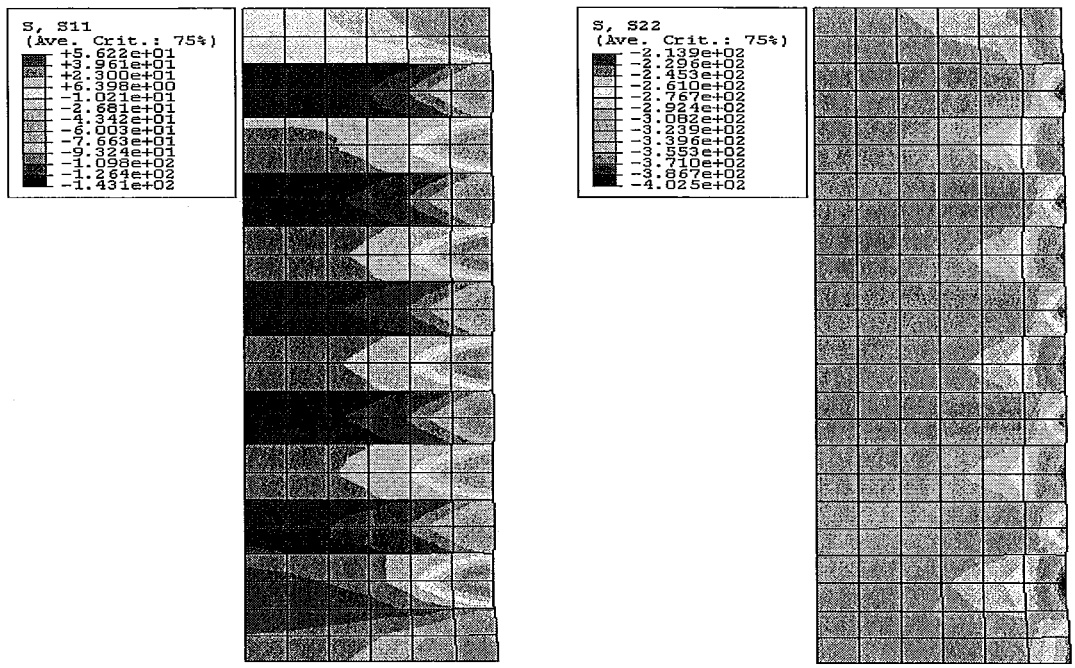

Fig. 4-4 FE simulation results on Sample B in an axial compression triaxial test; contours of vertical and horizontal stress in the deformed domain (deformation scale factor=5.0)

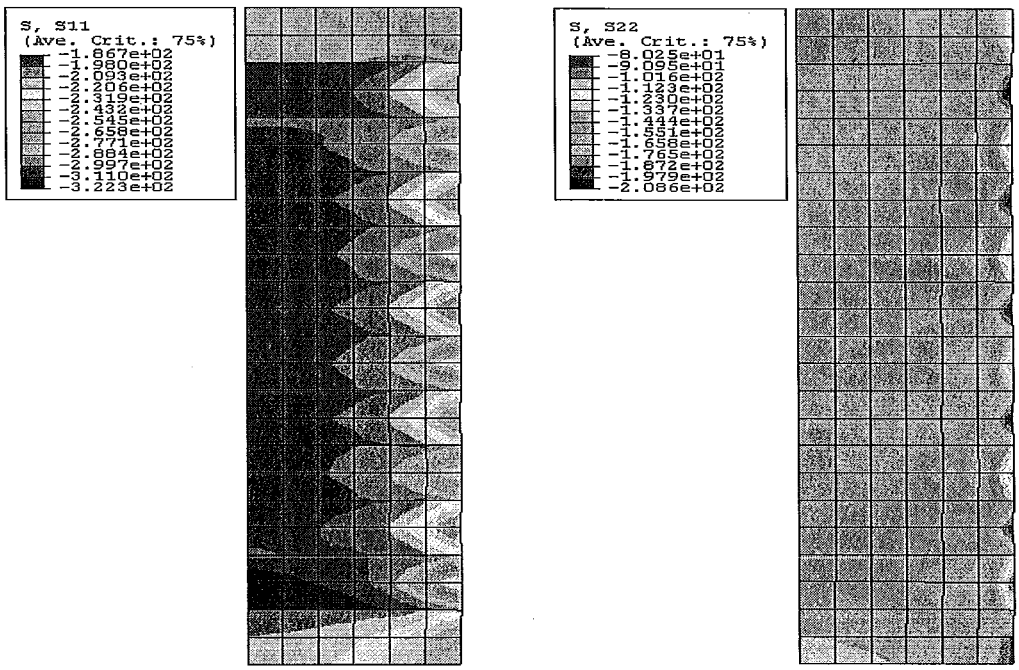

Fig. 4-5 FE simulation results on Sample B in a lateral compression triaxial test; contours of vertical and horizontal stress in the deformed domain (deformation scale factor=5.0)

CHAPTER 5

CONCLUSIONS AND RECOMMENDATIONS FOR FUTURE WORK

5.1 Summary and Conclusions

This study includes analytical, experimental and numerical aspects, and it provides an insight into the mechanical response of triaxial soil specimens consisting of numerous strata in the elastic range.

By using a homogenization technique it is shown that a system of strata can be replaced by an 'equivalent' homogeneous cross-anisotropic material. The elastic material properties of such an equivalent transversely isotropic were derived analytically, using the elastic constants of the constituents.

In the experimental program, samples consisting of layers of two different types of materials were tested in a triaxial apparatus to investigate and validate the assumption of equivalent transversely isotropic material. Layered samples were prepared in 6 and 12 layers, called Samples A and B respectively, using alternate layers of Dundas clay and kaolinite. In Phase I of the experimental investigation samples of Dundas clay, kaolinite and the layered system (Sample A) were tested in a triaxial apparatus to estimate the elastic range of their mechanical behavior. In Phase II, knowing the elastic range of the materials, the samples were tested in cyclic axial/lateral triaxial tests to find the elastic constants.

The observed behavior of the layered material and the constituents were analyzed and their elastic material properties were identified. Taking the elastic properties of Dundas clay and kaolinite from the experimental study and using them as inputs to the mathematical model, elastic constants of the layered system were evaluated analytically. The estimates of the elastic parameters from the analytical and the experimental studies of the equivalent transversely isotropic material were in a good agreement.

The stress-strain behavior of Samples A and B were also simulated using the finite element analysis. Once again the properties of the constituents were introduced as inputs. The predicted stress-strain characteristics of the layered system were examined and the elastic constants of the system were identified. The material properties of the equivalent transversely isotropic material found experimentally, analytically and numerically were compared to each other and were found to be in good agreement.

It has been demonstrated that a system of strata can be replaced by an 'equivalent' homogeneous cross-anisotropic .

5.2 Recommendations for Further Work

The experiments conducted in this study were only on samples with horizontal layers. Using a triaxial apparatus, the behavior of such systems with vertical layers should also be investigated. A more versatile test apparatus to investigate the behavior of anisotropic materials is the hollow cylinder device. Using this device the behavior of the material can be studied in various and complex stress states. Also the behavior of the material can be investigated under rotation of principal stresses with respect to material

axes, to experimentally examine the behavior for more complex loading histories. A study should also be carried out to identify the errors associated with the fabrication of non perfect samples.

REFERENCES

Backus G.E. (1962), Long-wave elastic anisotropy reduced by horizontal layering, J. Geophys. Res., Vol. 67, 4427-4440.

Brittan J., Warner M. and Pratt G. (1995), Anisotropic parameters of layered media in terms of composite elastic properties, Geophysics, Vol. 60, No. 4, 1243-1248.

Carcione J.M., Kosloff D. and Behle A. (1991), Long-wave anisotropy in stratified media: A numerical test, Geophysics, Vol. 56, 245-254.

Duveau G., Shao J.F. and Henry J.P. (1998), Assessment of some failure criteria for strongly anisotropic materials. Mech. Cohesive Frict. Mater., Vol. 3, No. 1, 1–26

Graham J. and Houlsby G.T. (1983), Anisotropic elasticity of natural clay, Geotechnique, Vol. 33, No. 2, 165-180.

Guo P. and Stolle D.F.E. (2009), Lower and upper limits of layered-soil strength, Can. Geotech. J., Vol. 46, No. 6, 665–678.

Kirkgard M.M. and Lade P.V. (1991), Anisotropy of normally consolidated San Francisco bay mud, Geotechnical Testing Journal, Vol. 14, No. 3, 231-246.

Lo K.Y. and Hori M. (1979), Deformation and strength properties of some rocks in southern Ontario, Canadian Geotechnical Journal, Vol. 16, No. 1, 108-120.

Melia, P.J. and Carlson R.L. (1984), An experimental test of P-wave anisotropy in stratified media, Geophysics Vol. 49, 364-378.

Niandou H., Shao J.F., Henry J.P. and Fourmaintraux D. (1997), Laboratory investigation of the mechanical behaviour of Tournemire shale, Int. J. Rock Mech. & Min. Sci., Vol. 34, No.1, 3-16.

Niemunis A., Karcher C. and Theile T. (2000), An averaging procedure for layered materials, Int. J. Numer. Anal. Meth. Geomech., Vol. 24, No. 10, 837-851.

Nishimura S., Minh N. A. and Jardine R.J. (2007), Shear strength anisotropy of natural London clay, Geotechnique, Vol. 57, No. 1, 49-62.

Oda M., Koishikawa I. and Higuchi T. (1978), Experimental study of anisotropic shear strength of sand by plane strain test, Soils and Foundations, Vol. 18, No. 1, 25-38.

Oka F., Kimoto S., Kobayashi H. and Adachi T. (2002), Anisotropic behavior of soft sedimentary rock and a constitutive model, Soils and Foundations, Vol. 42, No. 5, 59-70.

Postma G.W. (1955), Wave propagation in a stratified medium, Geophysics, Vol. 20, No. 4, 780–806.

Saada A.S. (1993), Elasticity; Theory and Applications, 2nd edition, published by Krieger Publishing Company, Pergamon Press Inc.

Salamon M.D.G. (1968), Elastic moduli of a stratified rock mass, International Journal for Numerical and Analytical Methods in Geomechanics, Vol. 5, 519–527.

Stolle D. and Guo P. (2007), A look at the use of an equivalent homogeneous medium. Canadian Geotechnical Journal, Vol. 44, No. 5, 507–519.

Timoshenko S.P. and Goodier J.N. (1970), Theory of Elasticity, McGraw-Hill.

Wardle L.J. and Gerrard C.M. (1972), Equivalent anisotropic properties of layered rock and soil masses, Rock Mechanics, Vol. 4, No. 3, 155-175.

Yamada Y. and Ishihara K. (1979), Anisotropic deformation characteristics of sand under three dimensional conditions, Soils and Foundations, Vol. 19, No. 2, 79-94.

Appendix

Uniform layer by layer samples prepared in Phase I and using thin layer of fine sand between layers in Phase II are illustrated in Fig.A-1.

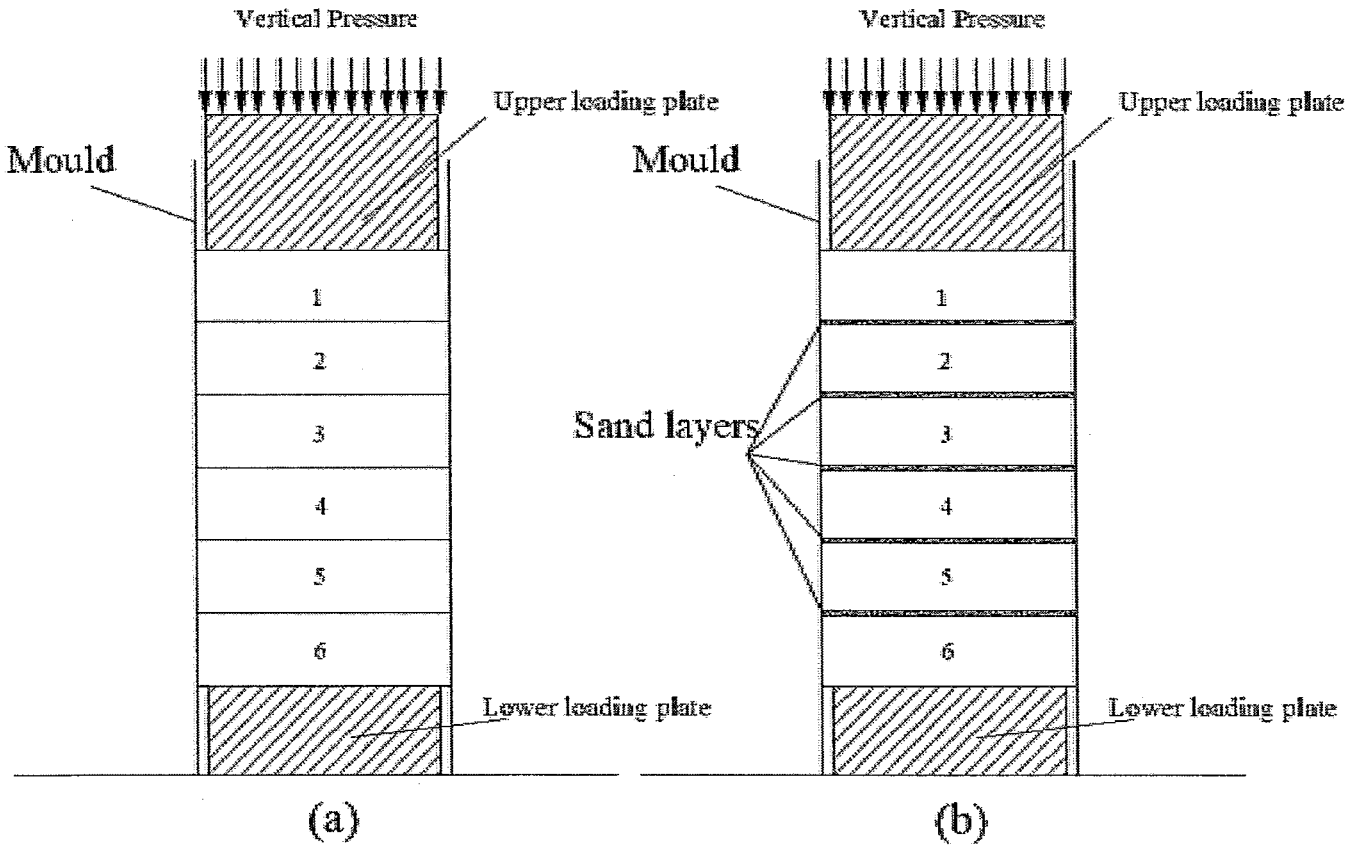

Fig. A-1 (a). Uniformly layer by layer samples preparation in phase I without sand layer (b). Sample preparation using a thin layer of sand in phase II

After testing each sample the water content was measured for every layer. For this purpose each layer was divided to a ring and core as shown in Fig. A-2.

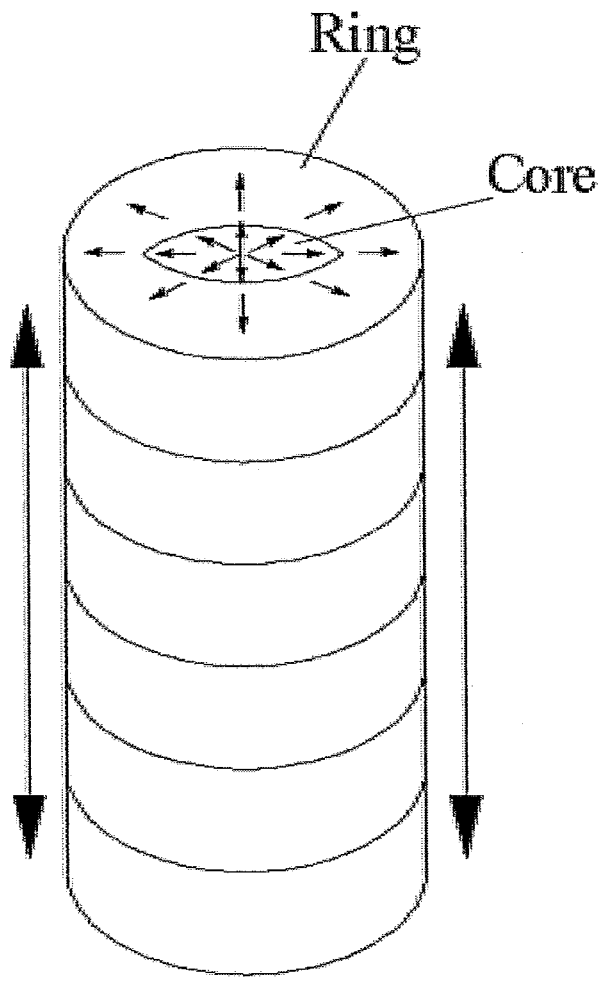

Fig. A-2 Water content flow from core to ring and to ends through the samples.

The water contents were measured separately for ring and core for each layers. The difference in water content distribution in both phases are shown in Table A-1 and Table A-2.

Table. A-1 Water content variations in the layers of Kaolnite in Phase I and Phase II

	Layer	Core	Ring	Variation		Layer	Core	Ring	Variation
Without Sand layers	1	14.43	17.63	3.21	With Sand layers	1	12.26	14.99	2.72
	2	11.76	14.37	2.61		2	12.12	14.81	2.69
	3	10.82	13.22	2.40		3	11.90	14.55	2.64
	4	10.10	12.34	2.24		4	11.76	14.37	2.61
	5	13.49	16.49	3.00		5	11.90	14.55	2.64
	6	15.87	19.39	3.53		6	12.48	15.25	2.77

Table. A-2 Water content variations in the layers of Brown clay in Phase I and Phase II

	Layer	Core	Ring	Variation		Layer	Core	Ring	Variation
Without Sand layers	1	12.55	15.34	2.79	With Sand layers	1	14.43	17.63	3.21
	2	12.40	15.16	2.76		2	11.76	14.37	2.61
	3	12.18	14.89	2.71		3	10.82	13.22	2.40
	4	12.03	14.71	2.67		4	10.10	12.34	2.24
	5	12.18	14.89	2.71		5	13.49	16.49	3.00
	6	12.77	15.61	2.84		6	15.87	19.39	3.53